

5 The Influence of Environment on Galaxy Evolution

Bernd Vollmer

Observatoire astronomique de Strasbourg, Strasbourg, France

1	<i>Introduction</i>	209
2	<i>Galaxy Populations in Groups and Clusters</i>	210
3	<i>Interaction Types</i>	211
3.1	Gravitational Interactions	211
3.2	Hydrodynamical Interactions	213
4	<i>Simulations</i>	215
4.1	Spherical Galaxies	216
4.2	Disk Galaxies	216
5	<i>The Multiphase ISM</i>	219
5.1	Atomic Hydrogen	219
5.2	Molecular Hydrogen	221
5.3	Dust and Metallicity	223
5.4	Cosmic Ray Gas	224
6	<i>Star Formation</i>	225
7	<i>The Global Picture</i>	226
8	<i>Resolved Multiwavelength Interaction Diagnostics</i>	231
8.1	Environmental Effects in Nearby Galaxy Groups	232
8.2	Environmental Effects in Nearby Galaxy Clusters	235
8.2.1	Early Type Galaxies	237
8.2.2	Late Type Galaxies	239
8.2.3	Dwarf Galaxies	245
8.3	A Holistic View on Ram Pressure Stripping	247
8.3.1	The Response of the Multiphase ISM and Star Formation to Ram Pressure	251

9 *The Detailed Picture* 253

10 *A Local View on the Butcher-Oemler Effect* 255

11 *Conclusions and Outlook* 257

Acknowledgments 258

References 258

Abstract: Galaxy evolution is influenced by environment. The properties in terms of morphology, color, gas content, and star formation of galaxies residing in the field, groups, or clusters are markedly different. Environmental effects include gravitational interactions with other galaxies or the cluster potential and hydrodynamical effects as ram pressure stripping. An overview of the theoretical and observational aspects of galaxy evolution in different environments is given. Spherical, disk, and dwarf galaxies are discussed separately. Different simulation techniques for the modeling of environmental effects on the ISM are presented and compared. Environmental interactions leave imprints on the atomic and molecular hydrogen, dust, cosmic ray gas, and large-scale magnetic fields. They also modify the star formation of a galaxy that enters an environment of higher density. A global picture of galaxy evolution in different environments is drawn by combining integrated and resolved observations at multiple wavelengths. Special attention is given to multiwavelength interaction diagnostics of individual cluster galaxies. This leads to a more detailed understanding where and how different interactions occur. We are now at the point where we can study the reaction (phase change, star formation) of the multiphase ISM (molecular, atomic, ionized) to environmental interactions.

1 Introduction

During cosmic evolution, matter, which is sufficiently close to a massive object, decouples from the Hubble flow and is accreted by the massive object. Accretion takes place mostly within filamentary structures. In this way, a galaxy cluster gains mass through infall of dark matter, gas, and stars. Galaxy clusters have typical masses of 10^{14} – $10^{15} M_{\odot}$ and sizes of several Mpc. They contain hundreds of galaxies. The mass budget is dominated by dark matter which contributes about 80% to the total mass; galaxy clusters are thus the objects with the highest dark matter fraction in the universe. A tenuous ($\sim 10^{-3} \text{ cm}^{-3}$) gas sits in the gravitational potential of the whole cluster. When gas falls into the galaxy cluster, accretion shocks heat it to the Virial temperature (10^7 – 10^8 K; Sarazin 1986). It then stays hot, because of the exceedingly long cooling time of such a low-density gas. This X-ray emitting cluster atmosphere represents typically 10–20% of the total cluster mass. The optically visible side of a galaxy cluster, i.e., the galaxies, only account for 5–10% of the cluster mass. The large-scale evolution of a galaxy cluster is thus mainly governed by gravitation and gas heating.

On smaller scales, things are more complex. Together with the dark matter and gas, galaxies fall into the cluster. These galaxies might have been isolated or assembled in groups before infall. Once they enter the cluster, their evolution can change radically through interactions with their environment. It is known for decades that galaxy populations in clusters are very different from those in the field, i.e., outside galaxy groups and clusters. The morphological type of a galaxy is closely related to its environment (Dressler 1980; Whitmore and Gilmore 1991): whereas about 80% of the field galaxies are spirals, this fraction drops to $\sim 50\%$ at the cluster outskirts and becomes almost zero in cluster cores.

Even within the disk galaxy population, cluster spiral galaxies are redder and have less star formation than field galaxy of similar Hubble types (Kennicutt 1983; Gavazzi et al. 2006a). Since morphology is closely related to the star formation history of a galaxy, it is not surprising that the average galaxy properties related to star formation also depend on local density (Hashimoto et al. 1998; Lewis et al. 2002; Gómez et al. 2003; Kauffmann et al. 2004; Balogh et al. 2004). The fraction of early-type galaxies and passive non-star-forming galaxies both grow with time

during cluster evolution. The rate at which these fractions change depends sensitively on environment, i.e., the local density of galaxies (Dressler et al. 1997; Poggianti et al. 1999; Smith et al. 2005; Postman et al. 2005; Moran et al. 2007). Whereas in the cluster cores the early-type fraction has increased steadily with time from 70% at $z = 1$ to 90% at the present epoch, in intermediate-density regions corresponding to groups and the accretion regions of rich clusters, significant evolution appears to begin only after $z = 0.5$. At the same time, the fraction of blue star-forming galaxies in clusters decreases with time (Butcher–Oemler effect; Butcher and Oemler 1978, 1984).

The analysis of a spectroscopic catalog of galaxies in ten distant clusters (Dressler et al. 1999; Poggianti et al. 1999) has shown that the galaxy populations of these clusters are characterized by the presence of a large number of post-starburst galaxies. Poggianti et al. (1999) concluded that the most evident effect due to the cluster environment is the quenching of star formation rather than its enhancement. They found two different galaxy evolution timescales in clusters: (i) a rapid halt of star formation activity (~ 1 Gyr) and (ii) a slow transformation of morphology (several Gyr).

To understand the galaxy transformation with time, we have to understand when, where, and which interaction between a galaxy and its cluster environment changes the galaxy's aspect. The ideal place to find answers to these questions is a local cluster where the interaction mechanisms can be studied in detail at high spatial resolution (≤ 1 kpc) and where the whole range of galaxies to low luminosities can be observed. Therefore, this chapter is focused on the Virgo, Coma, and Abell 1367 clusters and to a lesser extent, on the Norma and Fornax clusters. At this point, it should be noted that galaxy clusters can be very different. Whereas the Virgo cluster is a dynamical young cluster with a high spiral fraction and a peaked X-ray emission (cooling core cluster), the Coma cluster is more relaxed and spiral-poor and has a much more extended X-ray emission distribution.

The consequences of a galaxy–cluster interaction can be observed in the integrated and resolved properties of a cluster galaxy. The seminal article on late-type galaxy evolution in local clusters of Boselli and Gavazzi (2006) is mainly based on the integrated properties of cluster galaxies at multiple wavelengths. The fundamental review on the relation between physical properties and environment of Blanton and Moustakas (2009) is based on statistical results from recent large surveys of nearby galaxies including the SDSS. Therefore, special attention will be paid to the resolved properties of Virgo spiral galaxies.

2 Galaxy Populations in Groups and Clusters

As many as 50–70% of all galaxies reside in groups of galaxies (Eke et al. 2005). These groups contain less than ~ 100 galaxies and have total masses of $\sim 10^{13} M_{\odot}$. Studies of groups at low redshift have revealed them to be a heterogeneous population with their galaxy populations varying from cluster-like to field-like (Zabludoff and Mulchaey 1998). Groups showing extended X-ray emission tend to have a significant fraction of early-type galaxies and a dominant early-type galaxy at the group center (Mulchaey and Zabludoff 1998; Mulchaey et al. 2003; Osmond and Ponman 2004; Jeltema et al. 2007). About 30% of galaxy groups are dominated by elliptical or lenticular galaxies (Croston et al. 2005).

The group environment changes the morphology of galaxies. McGee et al. (2008) compared the fractional bulge luminosities of galaxies in groups at $0.3 < z < 0.55$ to a similarly selected

group sample at $0.05 < z < 0.12$. They found that, at both epochs, the group and field fractional bulge luminosity distributions differ significantly, with the dominant difference being a deficit of disk-dominated galaxies in the group samples. The group environment thus favors the formation of bulge-dominated early-type galaxies.

The same phenomenon is found in galaxy clusters. From his study of $\sim 6,000$ galaxies in 55 rich clusters, Dressler (1980) showed that the fraction of early-type galaxies increases with projected galaxy density: elliptical galaxies prevail in high-density regions, i.e., in the cores of massive clusters, whereas spiral galaxies are the dominant population in low-density regions. Lenticular galaxies occupy regions with intermediate to high galaxy densities. This is known as the morphology–density relation.

Moreover, the fraction of spiral galaxies in a galaxy cluster increases with increasing redshift (Dressler et al. 1997; Fasano et al. 2000). The spiral population in distant clusters consists of the great majority of blue galaxies responsible for the Butcher–Oemler effect, as well as a sizeable fraction of the red population (Dressler et al. 1999; Poggianti et al. 1999). Coupled to the increase in the spiral fraction, the S0 galaxies at intermediate redshifts are proportionately (two to three times) less abundant than in nearby clusters, while the fraction of ellipticals is already as large or larger (Dressler et al. 1997).

A morphology–density relation also exists for dwarf galaxies: dwarf elliptical galaxies are more frequent in dense environments, while dwarf irregulars are ubiquitous (Binggeli et al. 1990; Sabatini et al. 2005).

In galaxy clusters, a morphological segregation with respect to the distance from the cluster center is observed for $R < 0.5$ Mpc (Dressler 1980; Whitmore et al. 1993). Thomas and Katgert (2006) claimed that this morphology–radius relation is mainly due to the different radial distributions of bright elliptical and late-type galaxies.

Environment thus influences the morphological mix of galaxies in regions of different galaxy density and/or cluster radius. Is this mix already in place before the assembling of a massive structure as a galaxy cluster (nature) or is it established by galaxy evolution within a dense environment (nurture)? Environment does play an important role for the evolution of late-type spiral galaxies. In the following, it will be discussed how interactions between a galaxy and its environment can affect its ecology and ultimately its morphology.

3 Interaction Types

One can distinguish two different classes of interactions based on gravitation or gas physics. The first class includes galaxy–galaxy and galaxy–cluster tidal interactions. The second class involves the hot intracluster medium through which the galaxy is moving at a high speed. Whereas gravitational interactions act in the same way on all components of a galaxy (dark matter, stars, and gas), hydrodynamic interactions only affect the galaxy’s interstellar matter.

3.1 Gravitational Interactions

The tidal interaction of a galaxy and the *gravitational potential of the whole cluster* is compressive within the cluster core. A disk parallel to the orbital plane develops a transient spiral pattern. If the disk is inclined with respect to the orbital plane, it is transiently compressed and

an initially circular disk is deformed into an ellipse (Byrd and Valtonen 1990; Valluri 1993; Henriksen and Byrd 1996). The compression increases with decreasing distance to the cluster center.

Direct *galaxy–galaxy encounters* affect a spiral galaxy significantly if the impact parameter is of the order of or smaller than

$$b = r \left(2 \frac{M}{m} \right), \quad (5.1)$$

where r and m are the size and mass of the galactic disk at the optical radius and M is the mass of the perturbing galaxy. In addition, the relative velocity between the galaxy has to be close to the rotation velocity of the spiral galaxies ($100\text{--}200 \text{ km s}^{-1}$). The prominent example for a tidal interaction in the Virgo cluster is NGC 4438 (► Fig. 5-1).¹

Fast encounters with relative velocities much larger than the rotation velocity lead to tidal shocks, which heat the systems. The increased kinetic energy causes the system to expand and cool. A prograde encounter where the orbital angular momentum is aligned with the rotational angular momentum leads to strong tidal arms, whereas a retrograde encounter gives rise to only mild tidal distortions. The seminal article of Struck (1999) gives a detailed description of tidal effects during galaxy–galaxy encounters.

Since the velocity of cluster galaxies is large ($400\text{--}1,000 \text{ km s}^{-1}$), slow galaxy–galaxy encounters are rare once a galaxy has entered the cluster core. However, since a significant fraction of infalling galaxies are assembled in groups, slow encounters can occur at the periphery of clusters (preprocessing, Dressler 2004). On the other hand, multiple tidal shocks induced by rapid flybys of massive galaxies lead to an expansion of the stellar disk. This effect is termed *galaxy harassment* (Moore et al. 1996, 1999). The probability of close encounters with massive galaxies is higher in the cluster core, where the galaxy density is highest. The disk stars and gas loosened from the galaxy by multiple flybys are then stripped by the gravitational potential of the



■ Fig. 5-1
SDSS *gri* image of the NGC 4438/4435 system in the Virgo cluster

¹The strength parameter for a galaxy–galaxy collision has been defined by Gerber and Lamb (1994) as $S = 2GM/(bv_{\text{rel}}v_{\text{rot}})$, where v_{rel} is the relative velocity between the two galaxies and v_{rot} is the rotation velocity of the primary galaxy.

whole cluster. Since it is easier to strip matter from a galaxy with a shallow potential well, galaxy harassment most efficiently affects low-mass systems and might lead to a morphological transformation. However, in most cases harassment does not change the morphology of massive, high surface brightness disk galaxies (Moore et al. 1999).

Tidal shocking through multiple nearby high-speed encounters and the cluster potential depends on the galaxy orbit within the cluster. A highly eccentric orbit leads the galaxy close to the cluster center where both effects are strong.

3.2 Hydrodynamical Interactions

Whereas gravitational interactions act equally on the dark matter, stellar, and gaseous content of a spiral galaxy, hydrodynamical interactions take place between the hot intracluster gas and the interstellar medium of the galaxy. There is evidence that the star formation rate of a massive spiral galaxy of about $1 M_{\odot}/\text{year}$ has to be balanced by accretion of cold gas (Sancisi et al. 2008) and hot gas (Rasmussen et al. 2009) from an extended halo. In the absence of this gas halo, star formation is consuming the interstellar medium within a few Gyr. Larson et al. (1980) were the first to propose a halt of external gas accretion in cluster spiral galaxies. Bekki et al. (2002) developed this concept of *starvation* or *strangulation* by studying the stripping of an extended diffuse gas halo by ram pressure from the intracluster medium. They concluded that the diffuse halo is stripped if the galaxy orbit is eccentric, leading it to a pericenter distance three times larger than the cluster core radius. Once the halo is stripped, star formation will decrease and the galaxy becomes red.

A galaxy which enters a cluster on an eccentric orbit accelerates due to the gravitational potential of the cluster. At the same time, it encounters an intracluster medium of increasing density when it approaches the cluster center. From the point of view of the galaxy, which moves at a high speed through the cluster atmosphere, a wind due to ram pressure blows on its interstellar medium. If this ram pressure wind is higher than the gravitational restoring force due to the stellar disk, the gas is removed or stripped from the galactic disk (Gunn and Gott 1972):

$$\rho_{\text{ICM}} v_{\text{gal}}^2 > 2\pi G \Sigma_{*} \Sigma_{\text{ISM}} \sim \frac{v_{\text{rot}}^2}{R_{\text{str}}} \Sigma_{\text{ISM}}, \quad (5.2)$$

where G is the gravitation constant, ρ_{ICM} the intracluster medium density, v_{gal} the galaxy velocity with respect to the intracluster medium, $\Sigma_{*/\text{ISM}}$ the stellar/gas surface density, v_{rot} the rotation velocity, and R_{str} the stripping radius. Gas which is located at $R > R_{\text{str}}$ is removed via momentum transfer from the galactic disk by *ram pressure stripping*. The associated timescale is short $t_{\text{rps}} \sim 10\text{--}100$ Myr (Abadi et al. 1999; Vollmer et al. 2001a; Roediger and Brüggén 2006). One of the best examples of ongoing ram pressure stripping is the Virgo cluster spiral galaxy NGC 4522 (► Fig. 5-2).

Whereas momentum transfer ram pressure stripping only removes the gas of the outer disk, continuous gas removal from the whole gas disk proceeds via viscous stripping (Nulsen 1982). This stripping mode dominates if the galaxy moves edge-on through the cluster atmosphere. Viscosity can be classical for laminar flows or turbulent depending on the effective Reynolds number of the hot gas

$$Re = 2.8 \left(\frac{r_{\text{gal}}}{\lambda_{\text{ICM}}} \right) \left(\frac{v_{\text{ISM}}}{c_{\text{ICM}}} \right), \quad (5.3)$$

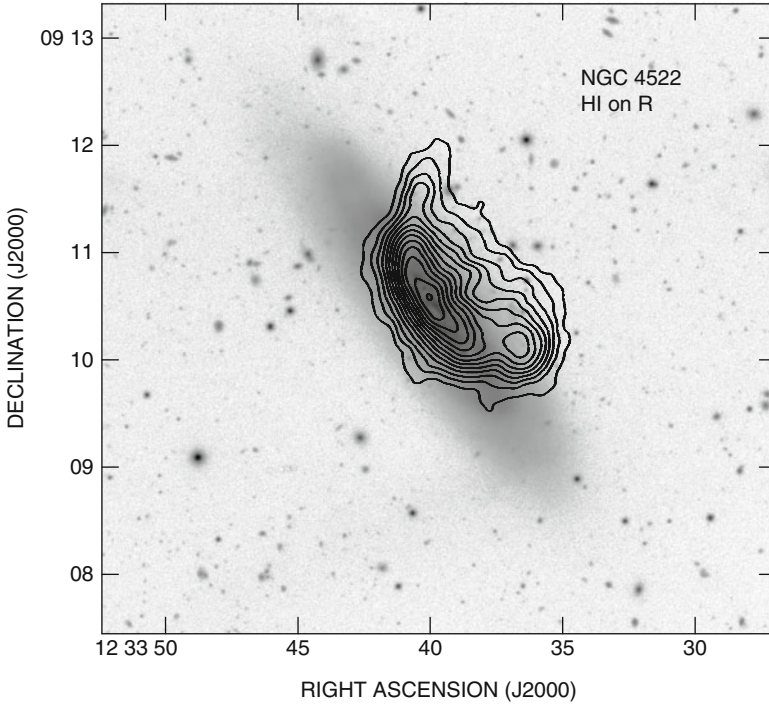


Fig. 5-2 The ram pressure stripped Virgo cluster spiral galaxy NGC 4522. *Grayscale*: stellar disk in the R-band image. *Contours*: HI surface density (From Kenney et al. 2004)

where λ_{ICM} is the characteristic length scale of the intracluster medium viscosity and c_{ICM} is the sound speed of the intracluster medium. If the characteristic length scale is the mean free path of ions in the intracluster medium,

$$\lambda_{\text{ICM}} \sim 11 \left(\frac{T_{\text{ICM}}}{10^8 \text{ K}} \right) \left(\frac{10^{-3} \text{ cm}^{-3}}{n_{\text{ICM}}} \right) \text{ kpc}, \quad (5.4)$$

where n_{ICM} is the number density of the intracluster medium. If $Re \geq 30$, the flow is expected to be turbulent. Turbulence is generated by Kelvin-Helmholtz instabilities at the interface between the intracluster and the interstellar medium. The gas disk which is not stripped by ram pressure is stable against Rayleigh-Taylor instabilities (Roediger and Hensler 2008). The mass loss rate in the two cases are

$$\dot{M}_{\text{laminar}} = 4.3\pi r_{\text{gal}} \rho_{\text{ICM}} \lambda_{\text{ICM}} c_{\text{ICM}} \quad \text{and} \quad \dot{M}_{\text{turb}} = \pi r_{\text{gal}}^2 \rho_{\text{ICM}} v_{\text{gal}}. \quad (5.5)$$

Both gas stripping rates are similar. The timescale of turbulent viscous stripping is

$$\tau_{\text{visc}} = \frac{\dot{M}_{\text{turb}}}{\dot{M}_{\text{ISM}}} \sim \frac{\rho_{\text{ISM}} H}{\rho_{\text{ICM}} v_{\text{gal}}} \sim \frac{\Omega v_{\text{turb}}}{\pi G \rho_{\text{ICM}} v_{\text{gal}}}, \quad (5.6)$$

where the ISM density is $\rho_{\text{ISM}} \sim \Omega^2/(\pi G)$ (Vollmer and Beckert 2002), Ω the angular velocity of the ISM, H the ISM disk height, and v_{turb} the velocity dispersion of the ISM. The critical ram pressure for turbulent viscous stripping is

$$\rho_{\text{ICM}} v_{\text{gal}}^2 > \rho_{\text{ISM}} \frac{\lambda_{\text{KH}} v_{\text{rot}}^2}{2\pi R_{\text{str}}} = \frac{\lambda_{\text{KH}} v_{\text{rot}}^2}{2\pi H R_{\text{str}}} \Sigma_{\text{ISM}}, \quad (5.7)$$

where λ_{KH} is the dominant wavelength for the gas ablation by Kelvin-Helmholtz instability (see, e.g., Mori and Burkert 2000). For $\lambda_{\text{KH}} \sim 6H$, this criterion is similar to the classical Gunn and Gott criterion (5.2). The stripping radius for viscous edge-on stripping is somewhat larger but comparable to that of momentum transfer face-on stripping (Marcolini et al. 2003). The instabilities lead to mixing of the intracluster medium into the ISM, which leads to a decrease of the ISM density. For $n_{\text{ICM}} = 10^{-4} \text{ cm}^{-3}$, $\Omega = 10^{-8} \text{ year}^{-1}$, $v_{\text{turb}} = 10 \text{ km s}^{-1}$, and $v_{\text{gal}} = 1,000 \text{ km s}^{-1}$, the viscous stripping timescale is $\tau_{\text{visc}} \sim 3 \text{ Gyr}$, much longer than that of classical momentum transfer ram pressure stripping (10–100 Myr). The magnetic fields contained in the ISM and intracluster medium might suppress Kelvin-Helmholtz instabilities (Landau and Lifshitz 1960; Spitzer 1978) and stripping might become laminar. Moreover, if the fields are stretched along the surface, thermal conduction will be suppressed (Vikhlinin et al. 2001).

4 Simulations

Since the work of Toomre and Toomre (1972), gravitational interactions between two galaxies have been simulated extensively (see, e.g., Combes et al. 1988; Barnes and Hernquist 1996; Duc et al. 2004). Today's simulations of gravitational interactions include the interstellar medium of the galaxies and a recipe for star formation. Byrd and Valtonen (1990) and Valluri (1993) investigated gravitational interactions between a disk galaxy and the gravitational potential of the whole cluster. Since the impact of this interaction on a galaxy is small, this subject did not receive further attention.

In the recent past, most progress has been made on the modeling of ram pressure stripping events. Therefore, this section is focused on the simulations of the hydrodynamic interaction between the intracluster medium and the ISM. The ISM can be simulated either by a continuous description (Eulerian hydrodynamics in 2D or 3D), a discrete description (sticky particles), or a discrete-continuous hybrid description (smoothed particles hydrodynamics, SPH). The common point of all methods is that the gas is treated as a collisional phase, whereas dark matter and stars are collisionless. The discrete description has no shocks nor instabilities and a finite penetration length of the intracluster medium into the ISM. This penetration length is 0 by definition in SPH. The latter method handles shocks and Rayleigh-Taylor instabilities, but it is not able to produce Kelvin-Helmholtz instabilities. The continuous description solves Euler's equations for compressible gas dynamics. Either the gas is assumed to be adiabatic or gas cooling is explicitly implemented. Modern codes contain an adaptive mesh refinement to resolve small-scale structures as shocks (see, e.g., Fryxell et al. 2000). Since the ISM is neither a continuous medium nor exclusively made of clouds, one has to choose the numerical method which is well adapted for the investigated astrophysical problem.

4.1 Spherical Galaxies

The bulk of gas in elliptical galaxy is hot, has a high volume filling factor, and can be detected in X-rays. It has to be modeled by a continuous prescription. The gas is supported against gravity by thermal pressure and rotation is negligible. Complete ram pressure stripping from a spherical galaxy requires that ram pressure exceeds the thermal pressure at the center of the gravitational potential well of the galaxy. For incomplete stripping, hydrodynamical simulations show a leading bow shock and a weak gravitationally focused wake or tail behind the galaxy.

Takeda et al. (1984), Gaetz et al. (1987), and Balsara et al. (1994) studied the influence of constant ram pressure in 2D. The two latter simulations included gas cooling and replenishment by stellar mass loss. Gaetz et al. (1987) determined several important parameters affecting the stripping efficiency. For not too high galaxy velocities, Balsara et al. (1994) found that the galaxy accretes mass from the downstream side into the core. Stevens et al. (1999) continued the work of Balsara performing a parameter study, for parameters appropriate for different clusters, ranging from cool clusters or groups up to hot clusters. They provide synthetic flux and hardness maps, as well as surface brightness profiles which can be directly compared to observations. Mori and Burkert (2000) studied ram pressure stripping of a cluster dwarf spheroidal galaxy without cooling and gas replenishment. They found that the gas in dwarf galaxies is rapidly removed in a typical cluster environment by ram pressure stripping. Stripping proceeds in two phases: (i) instantaneous ram pressure stripping via momentum transfer and (ii) gas ablation by Kelvin-Helmholtz instabilities with a timescale of ~ 1 Gyr.

4.2 Disk Galaxies

The ISM in disk galaxies is supported by rotation. For a face-on ISM-intracluster medium interaction, gas stripping occurs mainly via rapid momentum transfer. For edge-on interactions, slow viscous stripping or gas ablation by Kelvin-Helmholtz instabilities is responsible for ISM removal. For intermediate angles between the disk plane and the direction of the ram pressure wind, both mechanisms are at work. Since SPH and sticky particle codes do not produce Kelvin-Helmholtz instabilities, they cannot simulate turbulent viscous stripping.

All simulations validate the Gunn and Gott formula (► 5.2) and yield similar short timescales for ram pressure stripping via momentum transfer (10–100 Myr; Jáchym et al. 2007, 2009). Whereas sticky particle and SPH simulation produce similar results, Eulerian hydrodynamical simulations show differences in (i) the dependence between the stripped mass fraction and inclination angle between the disk plane and ram pressure wind and (ii) gas back-fall after the ram pressure peak. In the following, an overview is given on simulations using the different numerical techniques.

Tosa (1994) studied the influence of ram pressure on a disk galaxy treating the gas as test particles. Vollmer et al. (2001a) used a sticky particle code including the effects of ram pressure stripping to study the influence of (i) time-dependent ram pressure due to the galaxy orbit within the cluster and (ii) the inclination angle between the orbital and the disk plane on gas removal. They showed that ram pressure can lead to a temporary increase of the central gas surface density. In some cases, a considerable part of the total atomic gas mass (several $10^8 M_{\odot}$) can fall back onto the galactic disk after the stripping event. A quantitative relation between the orbit parameters and the resulting gas loss was derived containing explicitly the inclination angle between the orbital and the disk plane. Jáchym et al. (2009) proposed an alternative and

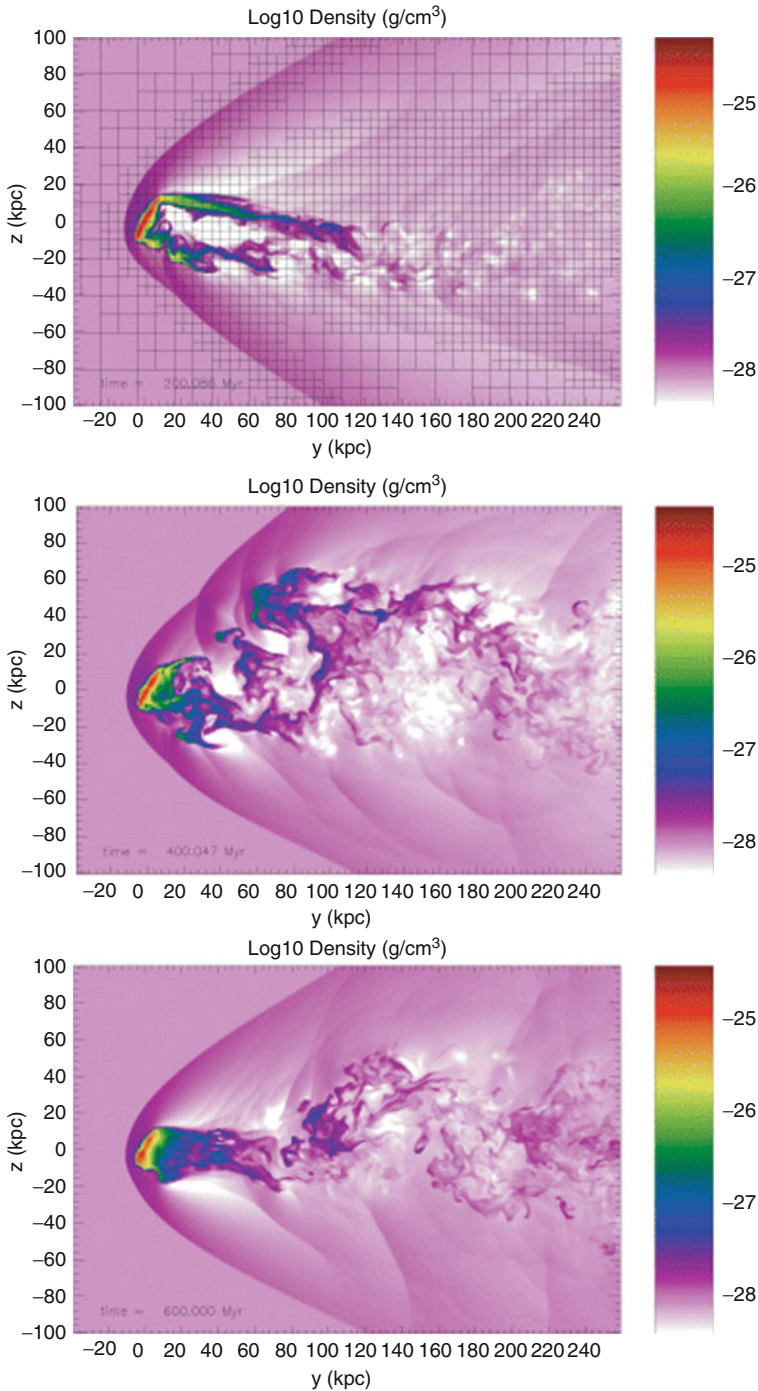
physically motivated relation depending on the disk tilt angle and on the column density of the encountered intracluster medium.

Abadi et al. (1999) modeled a constant ram pressure wind on a disk galaxy using SPH for different values of ram pressure and different inclination angles between the orbital and the disk plane. Schulz and Struck (2001) used an SPH code allowing for gas cooling. They observed a dependency of the stripped gas mass on the inclination angle. Not all the gas stripped from the disk escapes immediately from the halo, some gas can linger for times of order 100 Myr. Under the action of ram pressure, the gas disk is displaced relative to the halo center and compressed. In this way, the formation of numerous flocculent spirals is triggered. These waves transport angular momentum outward, resulting in further compression of the inner disk. This “annealing” process makes the inner disk, which contains much of the total gas mass, resistant to further stripping. Jáchym et al. (2007, 2009) investigated the evolution of the ISM which undergoes time-dependent ram pressure at various inclination angles with SPH. They highlighted the significant dependence of the stripping efficiency on the duration of a short ram pressure pulse. Their simulations confirmed the general trend of less stripping at orientations close to edge-on. The dependence on the disk tilt angle is more pronounced for compact intracluster medium distributions; however it almost vanishes for strong ram pressure pulses. The role of ram pressure stripping on star formation was studied by Kronberger et al. (2008).

Eulerian hydrodynamical simulations of ram pressure stripping of disk galaxies became possible only in the last decade in 2D (Roediger and Hensler 2005) and 3D (Quilis et al. 2000; Roediger and Brüggen 2006; Tonnesen and Bryan 2009). Marcolini et al. (2003) addressed the role of ram pressure stripping for dwarf disk galaxies. Roediger and Brüggen (2006) investigated the role of inclination between the orbital and the disk plane for constant ram pressure (► Fig. 5-3). They found that the inclination angle does not play a major role for the mass loss as long as the galaxy is not moving close to edge-on ($i > 30^\circ$). This different behavior compared to sticky particles and SPH is probably due to the action of strong Kelvin-Helmholtz instabilities. The stripping of disk galaxies on realistic orbits within the cluster was studied by Roediger and Brüggen (2007). These authors observed a repeated backfall of stripped gas prior to pericenter passage. In contrast to SPH and sticky particle simulations, there is no backfall after pericenter passage. Tonnesen and Bryan (2009) included radiative cooling in their high-resolution simulations to model the reaction of clumpy ISM to ram pressure stripping. In their simulations, lower density gas is stripped quickly from any radius of the galaxy, and the higher density gas can then be ablated via Kelvin-Helmholtz instabilities. The overall stripping timescale is thus longer than in previous simulations. The stripped gas tails are studied in Roediger et al. (2006), Roediger and Brüggen (2008), Tonnesen and Bryan (2010), and Tonnesen et al. (2011).

The combined influence of tidal interactions and ram pressure stripping was addressed by Vollmer (2003), Vollmer et al. (2005a, b), and Kapferer et al. (2008). Tidal interactions can push the outer ISM to larger galactocentric radii. In addition, the ISM has often a lower surface density. This tidally loosened gas is easily stripped by ram pressure. Tidal interactions thus increase the stripping efficiency.

Three-dimensional Eulerian hydrodynamic simulations of a whole galaxy cluster are presented in Domainko et al. (2006), Kapferer et al. (2007), and Tonnesen et al. (2007). These simulations generally show huge gas tails behind the stripped galaxies. In these simulations, the intracluster medium is not static but moving. Depending on the galaxy’s velocity vector \vec{v}_{ICM} , this changes ram pressure from $\rho_{\text{ICM}}v_{\text{gal}}^2$ to $\rho_{\text{ICM}}|\vec{v}_{\text{gal}} - \vec{v}_{\text{ICM}}|^2$. This can have significant consequences for a galaxy moving against the ram pressure wind (see NGC 4522 in ► Sect. 8.3).



■ Fig. 5-3

Three-dimensional Eulerian hydrodynamic simulation of a ram pressure stripping event. The local gas density is shown color-coded for different time-steps: *top* figure corresponds to a time of 200 Myr, the *middle* one to 400 Myr, and the *bottom* one to 600 Myr (From Roediger et al. 2006)

5 The Multiphase ISM

In a widely accepted picture (see, e.g., Kulkarni and Heiles 1988; Spitzer 1990; McKee 1995), the ISM consists of five different phases which are listed in [Table 5-1](#). About 80% of the total gas mass is neutral and 50% is in form of clouds or filaments. The warm/cold neutral phase is observable in H I line emission/absorption and the molecular phase in CO line emission. H α emission traces the dense warm ionized medium (diffuse gas and H II regions) and X-ray emission the hot ionized gas phase. The CO emission in spiral galaxies is concentrated in the inner disk where giant molecular clouds are ubiquitous. In field spiral galaxies, H α emission is detectable over the whole stellar disk. The extent of H I emission is usually 1.5–2 times larger than the galaxy’s optical diameter (R_{25}). Cosmic ray electrons, which are accelerated in supernova shock waves to relativistic velocities, are observable in the radio continuum at wavelengths ≥ 6 cm. The associated magnetic field is traced by the polarized radio continuum emission. In the following, an overview is given on the observations of the different ISM phases in groups and clusters with emphasis on nearby clusters.

5.1 Atomic Hydrogen

The ISM at galactic radii larger than ~ 2 scale-lengths of the optical disk of a spiral galaxy is mostly made of atomic hydrogen. The H I disk of isolated galaxies typically extends up to 1.5–1.8 optical radii (Cayatte et al. 1990; Salpeter and Hoffman 1996; Broeils and Rhee 1997; Walter et al. 2008). Since the outer gas of a spiral galaxies is less strongly bound by the gravitational potential, it is most vulnerable against external perturbations. Therefore, the H I emission of a cluster and group spiral galaxy is the most sensitive tracer of environmental interactions.

H I-deficient galaxies are observed in group environments. This indicates that the environment affects the gas content of the group galaxies. Since the galaxy velocity dispersion and the intragroup gas density are small, slow tidal interactions are the main driver of galaxy evolution within groups. The fraction of H I-deficient galaxies depends on the evolutionary stage of the group. Evolved groups display an X-ray halo and a high fraction of early-type galaxies. Kilborn et al. (2009) determined the H I deficiency of galaxies within 16 galaxy groups. They found that around two-thirds of H I-deficient galaxies were preferentially located at a

Table 5-1

The properties of the different phases of the ISM in spiral galaxies (From Boulares and Cox 1990)

	T (K)	n (cm^{-3})	$\langle n \rangle$ (cm^{-3})	v_{turb} (km s^{-1})	Φ_V	H (pc)	M/M_{tot} (%)
Hot ionized	$\sim 10^6$..	0.002	..	0.5	3,000	4
Warm ionized	$\sim 8,000$	0.3–10	0.025	~ 10	0.2	900	14
Warm neutral	$\sim 8,000$	0.1–10	0.1	~ 10	0.3	400	31
Cold neutral	~ 100	10–1,000	0.3	~ 6	0.02	140	25
Molecular	~ 10	>100	0.6	~ 6	0.001	70	26

T temperature, n : density, $\langle n \rangle$ mean density, v_{turb} dispersion velocity, Φ_V volume filling factor, H scale height, M/M_{tot} percentage of the total gas mass

projected distance of less than 1 Mpc from the group center.² Sengupta et al. (2007) observed 13 galaxies from four X-ray bright groups having disturbed and often truncated HI disks. Kern et al. (2008) imaged 16 HI sources in six galaxy groups. They found several interacting systems with extended HI envelopes. The Hickson compact groups (HCGs), owing to their high number density coupled with low-velocity dispersions, undergo frequent tidal interactions, distortions, and mergers between group members (Hickson et al. 1992; Mendes de Oliveira and Hickson 1994). Huchtmeier (1997) determined the HI content of 54 Hickson Compact groups. Many of these groups show extreme HI deficiencies as compared to nearby groups. In their sample of 72 Hickson compact groups, Verdes-Montenegro (2001) found that galaxies are, on average, deficient in HI by a factor of ~ 2 compared to loose groups. Tidal interactions between galaxies in groups thus can efficiently remove atomic gas from galactic disks.

Davies and Lewis (1973) were the first who noticed a difference in the HI content of Virgo spiral galaxies compared to field spiral galaxies of the same morphological type. A first quantitative comparison sample for isolated galaxies was established by Haynes and Giovanelli (1984). Similar to Chamaraux et al. (1980), these authors introduced the HI deficiency:

$$def_{\text{HI}} = \log \frac{M_{\text{HI}}^{\text{exp}}}{M_{\text{HI}}^{\text{obs}}}, \quad (5.8)$$

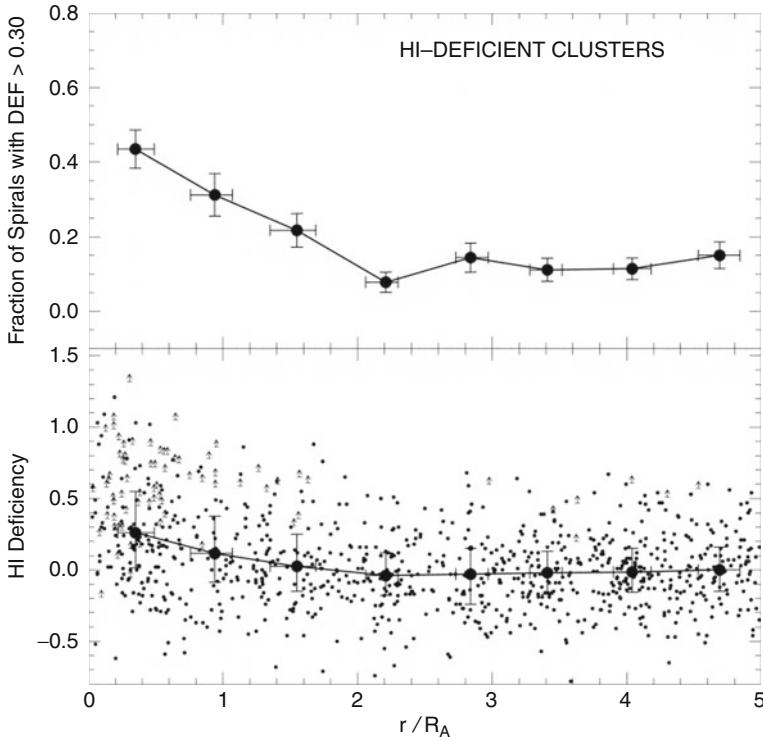
where $M_{\text{HI}}^{\text{obs}}$ is the observed and $M_{\text{HI}}^{\text{exp}}$ the expected HI mass of a galaxy of the same size and morphological type. A galaxy with an HI deficiency of $def_{\text{HI}} = 1$ has thus lost 90% of its atomic hydrogen. The typical uncertainty of the HI deficiency is 0.25. Based on their comparison sample, Giovanelli and Haynes (1985) showed that a significant fraction of galaxies in dense clusters are HI deficient and that the HI deficiency increases with decreasing distance to the cluster center (Fig. 5-4). Gavazzi (1987, 1989) and Gavazzi et al. (2005, 2006b) completed this picture for the Virgo cluster and the Coma supercluster region. The HI mass function of the Virgo Cluster differs significantly from that in the field, due to the combined effect of morphology segregation and the presence of HI-deficient objects (Gavazzi et al. 2005).

Solanes et al. (2001) continued the work of Giovanelli and Haynes (1985) by extending the sample to 1,900 galaxies within 18 clusters. They did not find a correlation between the fraction of HI-deficient spirals in a cluster and the clusters' global properties. The HI deficiency is related to the morphology of the galaxies and not to their optical size. The radial extent of the region with significant gas removal from galaxies can reach up to two Abell radii. Within this region, the fraction of HI-deficient spiral galaxies increases continuously toward the cluster center.

A blind Arecibo HI survey of the Virgo cluster (80 deg²) showed that HI-rich Virgo galaxies are structurally similar to ordinary late-type galaxies. This is consistent with a scenario where a structural change of a galaxies implies a significant loss of atomic hydrogen. Moreover, less than 1% of early-type galaxies contain neutral hydrogen ($>10^8 M_{\odot}$; Gavazzi et al. 2008).

Imaging observations of the atomic gas content of cluster spiral galaxies showed that HI-deficient galaxies have truncated gas disks (Virgo cluster: Warmels 1988; Cayatte et al. 1990; Chung et al. 2009 Fig. 5-5); Coma cluster: Bravo-Alfaro et al. 2000). Galaxies near the cluster core (≤ 0.5 Mpc) have HI disks that are significantly smaller compared to their stellar disks. The most natural explanation for these findings is ram pressure stripping. Cayatte et al. (1994) divided their galaxy sample into four groups: (i) HI-normal galaxies, (ii) galaxies with mildly truncated HI and a central surface density which is lower than that of normal galaxies, (iii) galaxies with strongly truncated HI and a low central surface density, and (iv) anemic galaxies

²Galaxy groups have sizes of ~ 1 Mpc. The typical size of compact groups is about half this value.



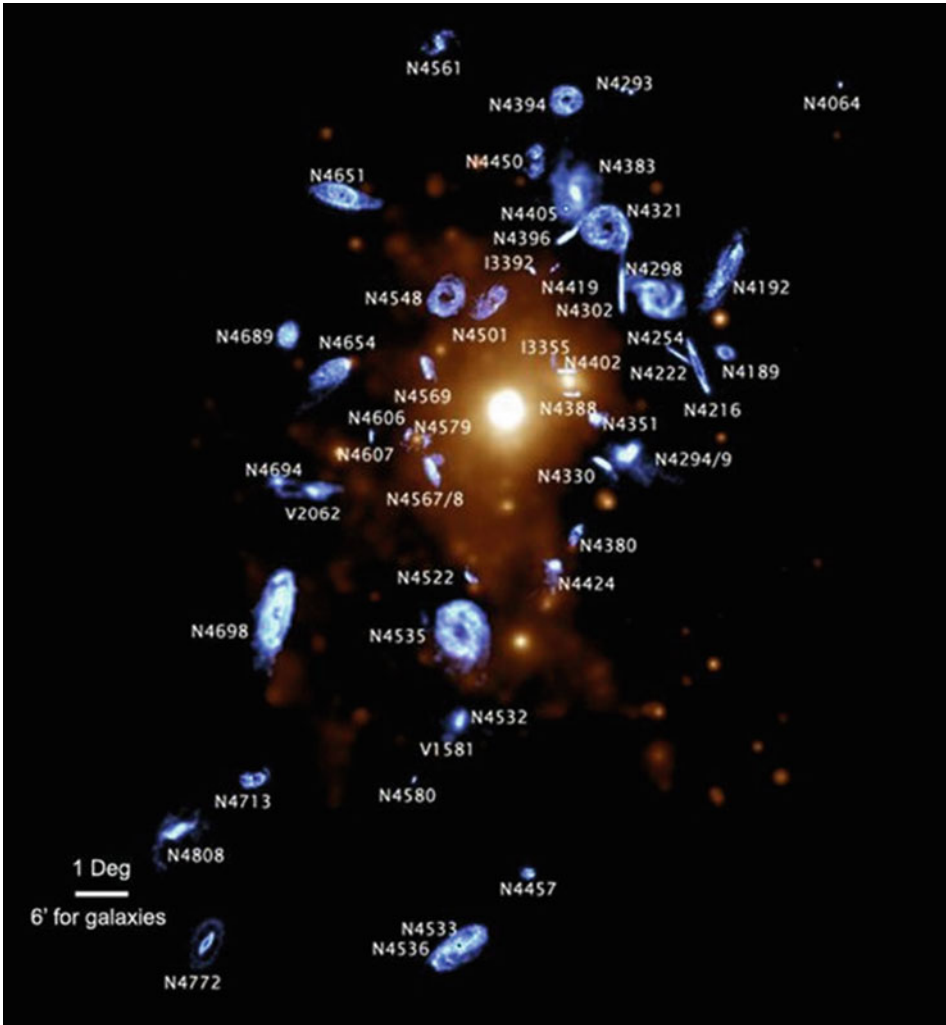
■ Fig. 5-4

Top: fraction of HI-deficient galaxies in bins of projected radius from the cluster center for the superposition HI-deficient clusters. Vertical error bars correspond to 1σ confidence Poisson intervals. The abscissae show medians and quartile values of the bins in radial distance. *Bottom*: Same as top panel for the measured HI deficiency. Displayed are the medians and quartiles of the binned number distributions in HI deficiency. *Small dots* show the radial variation of HI deficiency for individual galaxies, while the *arrows* identify non-detections plotted at their estimated lower limits (From Solanes et al. 2001)

which are mildly truncated and show an overall very low HI surface density. In their sample of ~ 50 Virgo galaxies, Chung et al. (2007) found seven spiral galaxies with long HI tails. These galaxies are found in intermediate- to low-density regions (0.6–1 Mpc in projection from M 87). The tails are all pointing roughly away from M 87, suggesting that these tails may have been created by a global cluster mechanism. A rough estimate suggests that simple ram pressure stripping could have indeed formed the tails in all but two cases. It should be noted that in three of the seven systems, a gravitational galaxy–galaxy interaction is involved.

5.2 Molecular Hydrogen

The ISM becomes mainly molecular in the inner part of the galactic disk. The H_2 surface density has about the same scale-length as the stellar disk (e.g., Leroy et al. 2008). The molecular



■ Fig. 5-5

Composite image of the H I distribution of the individual galaxies (in *blue*) overlaid on the ROSAT X-ray image (*orange*) by Böhringer et al. (1994). The galaxies are located at the proper position in the cluster, but each H I image is magnified by a factor 10 (From Chung et al. 2009)

gas is sitting deeply in the gravitational potential of the galaxy and is thus very hard to move or remove. However, in the absence of gas accretion, the molecular gas will be consumed by star formation within a few Gyr (Bigiel et al. 2008). Molecular hydrogen can only be indirectly observed via CO line emission. To derive H₂ column densities and masses, a conversion factor $X = N(\text{H}_2)/I(\text{CO})$ has to be assumed. For massive galaxies, the standard value $X = 2 \times 10^{20} \text{ cm}^{-2} (\text{K km s}^{-1})^{-1}$ applies (Dame et al. 2001). For low-mass, low-metallicity systems, the conversion factor is substantially higher. Boselli et al. (2002) give a correlation between

X and the NIR H band luminosity of a galaxy. As the HI deficiency, the H₂ deficiency is defined as the logarithm of the ratio between the expected and measured H₂ mass of a galaxy.

Observations of the molecular gas in group galaxies are rare. Boselli et al. (1996) did not find any difference between the molecular gas content of spiral galaxies in Hickson Compact groups compared to isolated spirals. On the other hand, Leon et al. (1998) argued for an enhanced molecular gas content in compact group galaxies, especially for the most compact groups, suggesting that tidal interactions can drive the gas component inward, and concentrating it in the dense central regions, where it is easily detected.

CO observations of galaxies in the Virgo (Stark et al. 1986; Kenney and Young 1986; Boselli et al. 1995, 2002) and Coma cluster (Casoli et al. 1991, 1996) did not show an H₂ deficiency in these clusters, i.e., cluster spirals are indistinguishable from field spirals with respect to their molecular gas content. However, Fumagalli and Gavazzi (2008) found a weak correlation between the H₂ mass divided by the stellar mass and the HI deficiency.

5.3 Dust and Metallicity

Heavy elements are produced in massive stars and released by stellar winds and supernova explosions. Metallicity is thus closely linked to the star formation history of a galaxy. The spectrum of a stellar population does not only depend on its age but also on its metallicity. Little is known about environmental effects on metallicity.

Early-type galaxies with low-velocity dispersions in Hickson Compact groups show an enhanced [Mg/Fe] ratio and depleted metallicity [Z/H] with respect to their counterparts in the field (de la Rosa et al. 2007). This anomalous behavior is interpreted as evidence for the action of a mechanism that truncates star formation. This is expected after a merger event between two spiral galaxies.

The influence of environment on metallicity is still an open question. Skillman et al. (1996) determined the metallicity gradients of 9 Virgo spiral galaxies. They found that HI-deficient Virgo galaxies have larger mean abundances than field galaxies of comparable luminosity or Hubble type, while the spirals at the periphery of the cluster are indistinguishable from the field galaxies. There is also weak evidence of shallower abundance gradients in the HI-deficient Virgo spirals compared to the spirals on the periphery of the cluster. On the other hand, by reanalyzing the Skillman sample, Pilyugin et al. (2002) found that all Virgo periphery and core spirals have counterparts among field spirals. They concluded that if there is a difference in the abundance properties of the Virgo and field spirals, this difference appears to be small and masked by the observational errors. Lee et al. (2003) compared oxygen abundances of Virgo to local dwarf elliptical galaxies with the conclusion that there is no systematic difference between the two populations. Boselli and Gavazzi (2006) presented evidence that HI-deficient galaxies have on average larger metallicities than similar objects with a normal gas content.

Metals are injected into the interstellar medium by AGB stars, stellar winds, and supernova explosions. These metals aggregate to form dust which absorbs the energy of the stellar UV emission and reemits it in the infrared. The ISM dust-to-gas column density ratio is related to the metallicity. Molecular hydrogen forms on the surface of dust grains. The H₂ formation timescale thus depends on the dust-to-gas ratio or metallicity of the ISM (Tielens and Hollenbach 1985). In normal galaxies, the bulk of dust mass has temperatures around 20 K and is detected at wavelengths >100 μm. The bulk of the radiation is emitted at wavelengths between 60 and 200 μm from warm dust (~30 K). Dust is mixed with the ISM and therefore follows

its distribution. Gas removal thus always implies dust removal. Bica and Giovanelli (1987) derived far-infrared (IRAS 60–100 μm) properties for a sample of over 200 galaxies in seven clusters. Irrespective of the H I deficiency of a cluster galaxy, the sample consists almost entirely of infrared-normal galaxies. However, they found a lack of high luminosity ($L_{\text{IR}} > 10^{11} L_{\odot}$) compared to the field. The Herschel (100–500 μm) Virgo cluster luminosity functions show the same lack of very luminous galaxies. In addition, they do not have the large numbers of faint galaxies seen previously in surveys covering less dense environments (Davies et al. 2010). Popescu et al. (2002) derived temperatures and masses of cold dust from the IRAS and ISOPHOT 170 μm data. Using the same data, Boselli and Gavazzi (2006) argued that there is a tentative trend of smaller dust masses in galaxies of higher H I deficiency. This is expected if the dust which is associated to the ISM is stripped during a ram pressure stripping event. Based on Herschel data, Cort ese et al. (2010b) confirmed this scenario by showing that galaxies with truncated H I disks also have truncated dust disks. Stickel et al. (2003) presented the first tentative detection of an intergalactic dust cloud in the region between galaxies near the stripped Virgo spiral galaxy, NGC 4402. The clearest evidence of dust displaced together with the ISM from the disk of the Virgo cluster spiral galaxy NGC 4438 is presented by Cort ese et al. (2010a).

5.4 Cosmic Ray Gas

Electrons are accelerated to relativistic velocities in supernova shocks. In the presence of a magnetic field, they emit synchrotron radiation. The hot electrons in H II regions emit thermal bremsstrahlung. The radio continuum emission of non-starburst galaxies at wavelengths >6 cm is dominated by synchrotron emission whose emissivity is proportional to the density of relativistic electrons and the magnetic field strength to the power of ~ 2 . In spiral galaxies, the radio continuum emission is closely related to the star formation rate and the far-infrared emission (Helou et al. 1985; Niklas et al. 1997; Niklas 1997). It is well possible that the influence of the cluster environment on the radio continuum emission of cluster galaxies depends on the cluster properties, especially on those of the intracluster medium. Jaffe and Gavazzi (1986), Andersen and Owen (1995), and Rengarajan et al. (1997) found an enhanced radio to far-infrared ratio in galaxies which are located in the cores of dense clusters. Gavazzi and Boselli (1999a) studied the radio luminosity function of Virgo cluster galaxies for early- and late-type galaxies separately. They found that late-type galaxies develop radio sources with a probability proportional to their optical luminosity, independently of their detailed Hubble type. In a second article, Gavazzi and Boselli (1999b) compared the radio luminosity functions of galaxies in different clusters to those of isolated galaxies. They concluded that the radio luminosity function of Virgo cluster galaxies is consistent with that of isolated galaxies, whereas the Coma cluster galaxies show an excess of radio emissivity. Moreover, Gavazzi and Boselli (1999b) suggested that the radio excess observed in dense cluster galaxies is probably due to ram pressure compression of the ISM and its associated magnetic field or shock-induced re-acceleration of relativistic electrons as proposed by V olk and Xu (1994). It should be kept in mind that in the absence of imaging observations, a radio excess can also be due to nuclear activity. Vollmer et al. (2004a) determined the spectral index of the radio continuum emission of 81 Virgo galaxies. They noted that galaxies showing flat radio spectra also host active centers. No clear trend appeared between the spectral index and the galaxy's distance to the cluster center.

6 Star Formation

As reviewed in [Chap. 3](#), the star-formation activity of a galaxy can be determined using various tracers (Kennicutt 1998a): (i) dense HII regions around massive ($>8 M_{\odot}$) stars give rise to H α line emission, (ii) other recombination and forbidden nebular lines are emitted by gas around massive stars, (iii) intermediate-mass ($2\text{--}5 M_{\odot}$) stars show strong UV emission, (iv) dust is heated by this UV emission and radiates at wavelengths between 15 and 60 μm , and (v) supernova shocks/remnants emit in the radio continuum. Since star formation approximately follows the ISM surface density via the Schmidt law (Schmidt 1963; Kennicutt 1998b), gas removal leads to a decrease of star formation in a group or cluster galaxy. On the other hand, gravitational interactions can lead to important tidal torques which compress the gas and lead to a temporarily enhanced star formation rate.

Wilman et al. (2005) showed that the fraction of galaxies with [O II] emission, a measure of star formation, is much higher in group galaxies at intermediate redshift ($z \sim 0.4$) than in the local universe. However, the group galaxies still exhibit suppressed star formation relative to the field at the same epoch. Although observations have found abundant traces of tidal interactions in Hickson Compact Group (HCG) galaxies (Mendes de Oliveira and Hickson 1994), their star formation levels are surprisingly similar to those found in isolated galaxies (e.g., Zepf and Whitmore 1991; Moles et al. 1994; Allam et al. 1996; Verdes-Montenegro et al. 1998; Iglesias-Páramo and Vílchez 1999). Johnson et al. (2007) looked at the Spitzer IRAC (3.6–8.0 μm) color space distribution of HCGs and found that the mid-infrared (MIR) colors of galaxies in H I gas-rich HCGs are dominated by star formation, while the MIR colors of galaxies in H I gas-poor HCGs are dominated primarily by stellar photospheric emission. Galaxies in the most gas-rich groups tend to be the most actively star forming. Galaxies in the most gas-poor groups tend to be tightly clustered around a narrow range in colors consistent with the integrated light from a normal stellar population. These authors infer an evolutionary sequence in which galaxies in gas-rich groups experience star formation and/or nuclear activity until their neutral gas is consumed, stripped, or ionized.

Kennicutt (1983) was the first to compare the star formation rate of cluster spirals to that of field spirals of similar Hubble type. He found that Virgo cluster spiral galaxies have on average lower star formation rates than their isolated counterparts. Based on H α observations of 273 galaxies in the Virgo, Coma, Abell 1367, and Cancer clusters, Gavazzi et al. (2006a) concluded that, within each Hubble-type class, galaxies with normal H I content have twice the H α equivalent width of their H I -deficient counterparts. The star formation rate per unit mass of high-luminosity spirals that are projected within one virial radius is about a factor of 2 lower than at larger clustercentric projected distances, whereas low-luminosity objects have similar H α properties at all clustercentric radii.

The analysis of the H α equivalent width of large galaxy samples with redshifts $0.03 \leq z \leq 0.1$ from the SDSS and the 2dF survey (Lewis et al. 2002; Gómez et al. 2003; Tanaka et al. 2004) showed that the overall distribution of star formation rates is shifted to lower values in dense environments compared with the field population. This is consistent with earlier findings by Hashimoto et al. (1998). The distribution of the star formation rate as a function of projected galaxy surface density shows a discontinuity or a break at a galaxy number density of $\sim 1 \text{ Mpc}^{-2}$. This corresponds to a cluster radius of about 4 Mpc or ~ 3 Virial radii. In the Tanaka et al. (2004) sample, only faint galaxies show this break. The morphology of these galaxies also changes significantly. It seems thus difficult to disentangle the star formation-density relation from the

morphology–density relation. It should be noted that all galaxies used in these samples are of high luminosity according to the definition of Gavazzi et al. (2006a).

Imaging observations of the star formation of larger samples of cluster galaxies are rare. Koopmann and Kenney (2004a, b) divided the H α morphology of 52 Virgo spiral galaxies into several categories: (i) normal (37% of the sample), anemic (6%), enhanced (6%), and (spatially) truncated (52%). Anemic galaxies have a significant lower overall H α surface brightness. Truncated galaxies are further subdivided on the basis of their inner star formation rates into truncated/normal (37%), truncated/compact (6%), truncated/anemic (8%), and truncated/enhanced (2%). The fraction of anemic galaxies is relatively small ($\sim 10\%$) both in the Virgo cluster and the field, suggesting that starvation is not a major factor in the reduced star formation rates of Virgo spiral galaxies. The majority of Virgo spiral galaxies have their H α disks truncated, whereas truncated H α disks are rarer in isolated galaxies (● Fig. 5-6). Most of the H α -truncated galaxies have relatively undisturbed stellar disks and normal to slightly enhanced inner disk star formation rates. Koopmann and Kenney (2004a, b) suggested that ram pressure stripping is the main mechanism causing the reduced star formation rates of Virgo spiral galaxies. Fumagalli and Gavazzi (2008) found in their much smaller Virgo cluster galaxy sample a larger fraction of truncated/anemic galaxies.

7 The Global Picture

Based on the observational findings presented in ● Sect. 5, a consistent global picture for galaxy evolution in groups and cluster can be constructed.

Since in galaxy groups, the galaxy velocity dispersion ($\sim 200 \text{ km s}^{-1}$) and the density of the intergalactic medium are low, ram pressure is in most cases negligible and slow galaxy–galaxy collisions should be the main driver of galaxy evolution. Close flybys leading to important tidal perturbations are relatively frequent. Tidal interactions can pull gas and stars out of the gravitational potential of a galaxy. In X-ray bright groups, which have a rich intergalactic medium, the tidally expelled gas might then be stripped by ram pressure. The merging of two spiral galaxies leads to a lenticular or elliptical galaxy, depending on the interaction parameters. The end product are galaxies with a quenched star formation which then evolve passively. Thus, group galaxies can already be gas deficient with a low star formation rate with respect to their field counterparts and/or of early type before they fall into a galaxy cluster. This phenomenon is termed as preprocessing of galaxies in groups. Cort ese et al. (2006) presented a nice illustration of a compact group with a bright lenticular galaxy which is falling into the galaxy cluster Abell 1367. If the low-luminosity group galaxies were observed later, when ram pressure has stripped their gas entirely and star formation has stopped, they would probably resemble the post-starburst galaxies detected by Poggianti et al. (2004) in the Coma cluster.

Once a galaxy enters the cluster, its fate depends on the eccentricity of its orbit and the distribution of the intracluster medium. Observations indicate that H I -deficient galaxies are on more eccentric orbits within a cluster than H I -normal galaxies (Dressler 1986; Solanes et al. 2001). Numerical simulations (Ghigna et al. 1998) showed that galaxy dark matter halos evolving within a cluster settle on isotropic orbits with a median ratio of pericentric to apocentric radii of 1:6. In dynamically young, spiral-rich clusters as Virgo, the intracluster medium distribution is peaked on the central elliptical galaxy. In relaxed, spiral-poor clusters such as Coma, the intracluster medium distribution is more extended. In the latter case, less eccentric orbits are

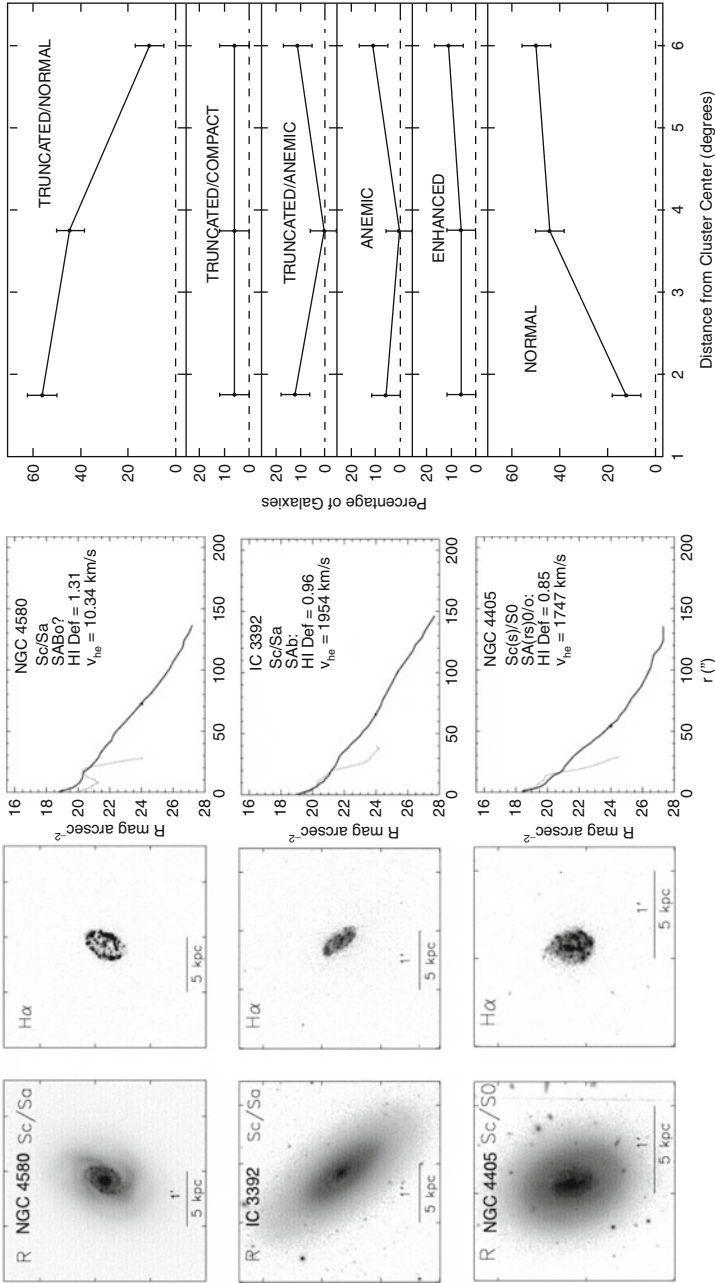


Fig. 5-6

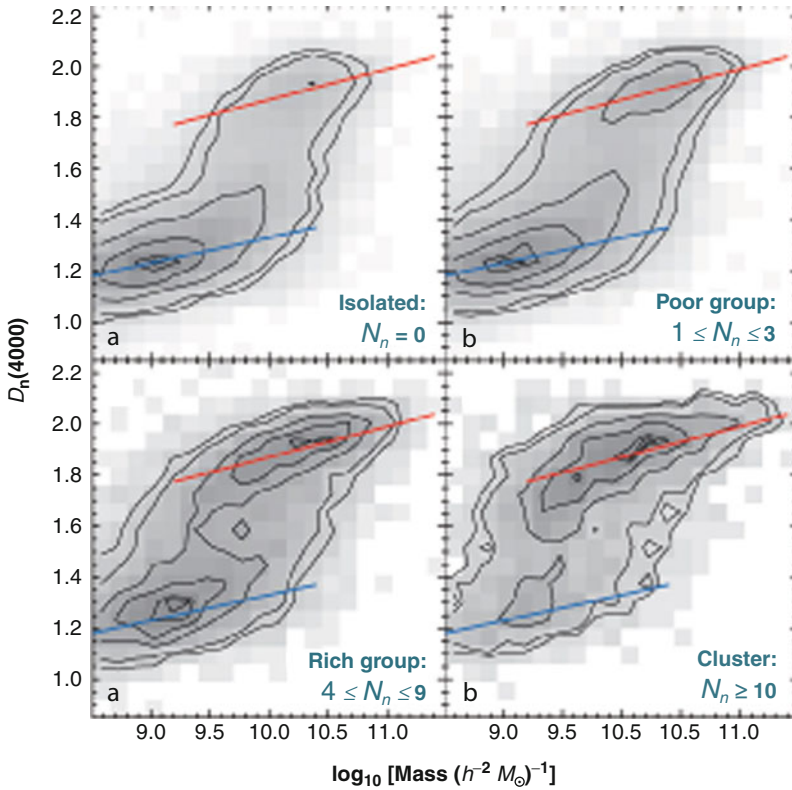
Left: R-band and H α images of three Virgo cluster galaxies with severely truncated star-forming disks. These galaxies have regular stellar disks, and their H α morphologies show symmetric rings of star formation near the truncation radius. Middle: H α and R-band radial profiles. Right: cluster radial distributions of each galaxy class, plotted as percentages of all the galaxies in that radial bin. Bins are $\leq 3^\circ$, $3^\circ - 4.5^\circ$, and $\geq 4.5^\circ$. There is a clear radial dependence for the normal and truncated/normal classes, with fewer normal and more truncated/normal galaxies closer to the cluster center. Other H α classes have a flatter distribution (but contain fewer sample galaxies; from Koopmann and Kenney (2004b))

needed to remove a significant amount of gas from the galaxy by ram pressure stripping. The velocity dispersion of cluster galaxies is typically higher than 500 km s^{-1} . In the cluster core, where the galaxy density is high, gravitational encounters occur in the form of rapid flybys. These lead only to significant distortions if the impact parameter is small. At the apocenter of a galaxy orbit, far away from the cluster center, a slow galaxy–galaxy encounter is not excluded. The primary effect of the cluster environment on a galaxy is the quenching of its star formation. If ram pressure is the cause of the quenching, the timescale is small (10–100 Myr). If the main cause for the halt of star formation are gravitational interactions, the timescale is much longer $\geq 1 \text{ Gyr}$. The high fraction of spiral galaxies with truncated gas and star formation disks indicates that ram pressure is an important environmental effect in the Virgo cluster. Once the galaxies have lost their outer gas disk, star formation stops in these regions. There is no direct observational evidence that ram pressure instantaneously alters the gas content of the inner disk in a significant way. The molecular gas contents and star formation rates of stripped galaxies are similar to those of unperturbed galaxies. After a few Gyr, the gas of the inner disk will be consumed by star formation and truncated gas, and star formation disk will become anemic.

In the absence of significant star formation, the galaxy's color becomes red and the luminosity-weighted mean stellar population age increases. For the galaxy population of the local universe, a change in the fraction between the number of blue young and red old galaxies can already be observed in regions of low galaxy density. As expected, this fraction decreases with increasing density. In cluster of galaxies, the fraction between the number of blue young and red old galaxies is reversed with respect to that of isolated galaxies. Old red galaxies are the dominant population in clusters (► [Fig. 5-7](#); Blanton and Moustakas 2009). At fixed morphological class according to light concentration, the distribution of stellar population ages strongly depends on environment. In contrast, galaxy–scaling relationships keep constant with environment, i.e., the distribution of galaxy morphologies does not depend strongly on environment once color is fixed (e.g., Bamford et al. 2008; Blanton and Moustakas 2009). Based on the analysis of large samples of nearby galaxies, it is claimed that environmental effects are relatively local. It appears that preprocessing of galaxies in groups is the main driver of these effects (Blanton and Moustakas 2009). However, this does not exclude that cluster environment can significantly affect infalling galaxies (see ► [Sect. 8.2](#)).

How can a spiral be transformed into a lenticular galaxy? Dressler (1980) showed that the bulge sizes and bulge-to-disk ratios of lenticular galaxies are systematically larger than those of spiral galaxies. Boselli and Gavazzi (2006) confirmed this result for the Virgo cluster. Christlein and Zabludoff (2004) excluded the generation of early-type galaxies (E/S0) by fading the disks of late-type galaxies. Under their assumptions, the bulge luminosities needed to be physically enhanced for such a transformation. Since ram pressure does not act on the stellar content of a spiral galaxy, only tidal interactions can lead to such an enhancement. Moreover, (i) the large scatter in the Tully–Fisher relation of Coma and Virgo cluster S0 galaxies in comparison to the known late-type spiral relation, together with the small zero-point offset, and (ii) the weak dependence of morphological segregation on galaxy density cannot be explained by an S0 formation through simple gas removal from spiral galaxies. Again, tidal interactions like slow encounters, minor mergers, or harassment are needed to transform spiral galaxies into lenticulars (Dressler and Sandage 1983; Neistein et al. 1999; Hinz et al. 2003).

Bright and faint lenticulars might not share the same history (Barway et al. 2009). Bright cluster and field lenticulars resemble ellipticals and bulges of early-type spirals suggesting that they may have formed at early epochs via major mergers or rapid collapse. Faint cluster lenticulars show systematic differences with respect to faint field lenticulars. These differences support



■ Fig. 5-7

Distribution of the stellar age measured by the 4,000 Å break (defined by Balogh et al. 1999) as a function of the stellar mass for different environments (defined according to the number of neighboring galaxies with $M_r - 5 \log_{10} h < -18.5$ within a projected radius of $500 h^{-1}$ kpc and a velocity of 600 km s^{-1}). The blue and red lines are references for the young and old galaxy populations (From Blanton and Moustakas 2009)

the idea that the bulge and disk components fade after the galaxy falls into a cluster, while simultaneously undergoing a transformation from spiral to lenticular morphologies (Barway et al. 2009; Boselli and Gavazzi 2006). It thus seems that, if one wants to look for the end product of spiral galaxy transformation in a galaxy cluster, one should have a look at faint cluster lenticulars.

Due to their shallow gravitational potential, dwarf galaxies are particularly vulnerable to environmental interactions. Gravitational interactions, most probably in form of galaxy harassment (► Sect. 3.1), can efficiently remove stars and gas from the outer parts of the galaxy and transform the galaxy's morphology. Ram pressure stripping (● Sect. 3.2) of dwarf irregular galaxies (dI) removes the gas, stops star formation, and makes the galaxy evolve passively.

The density morphology relation (► Sect. 2) extends to low-luminosity dwarf galaxies (Binggeli et al. 1988, 1990). *Early-type dwarf elliptical* (dE) galaxies strongly prefer dense

environments. They represent the numerically dominant galaxy population in nearby galaxy clusters and groups (Ferguson and Binggeli 1994). In galaxy groups, dEs are preferentially found near giant galaxies. One of the specific properties making dE/dS0s different from late-type dwarf irregular and spiral galaxies is the lack of interstellar medium (ISM) and, hence, ongoing star formation. Stellar populations of dE galaxies are remarkably different from those of giant early-type galaxies pointing out to differences in star formation histories and chemical evolution.

Most dE galaxies have compact nuclei with a whole range of sizes and central surface brightnesses (Côté et al. 2006). Based on their analysis of 413 Virgo cluster dwarf ellipticals, Lisker et al. (2007) divided their sample into nucleated and nonnucleated dEs depending on the presence of a strong nucleus compared to the galaxy's total luminosity. The nonnucleated dEs can show disk features like bars or spiral arms (also named dwarf S0 galaxies, dS0) and can have central star formation. Whereas the nucleated dEs have a centrally peaked distribution within the cluster-like giant elliptical and lenticular galaxies, the distribution of nonnucleated dEs shows no central clustering.

About half of the dEs are supported by rotation (van Zee et al. 2004a; Toloba et al. 2011). Based on the observed maximum rotation velocities, the rotating dwarf galaxies appear to follow the Tully–Fisher relation for gas-rich dwarf and spiral galaxies. No significant difference in dominant stellar populations between rotating and nonrotating dwarf elliptical galaxies (Geha et al. 2003; van Zee et al. 2004b) or between dEs with and without disks (Paudel et al. 2010) were found. The analysis of the color–magnitude relation of these objects led Lisker et al. (2008) to the conclusion that there must be multiple formation channels. Boselli et al. (2008) compared UV to radio centimetric properties of star-forming and quiescent Virgo dwarf galaxies to the predictions of multizone chemospectrophotometric models. The models include the quenching of star formation due to ram pressure stripping. These authors suggested that young, low-luminosity, high surface brightness star-forming galaxies such as late-type spirals are probably the progenitors of relatively massive dwarf ellipticals, while it is likely that low surface brightness Magellanic irregulars evolve into very low surface brightness quiescent objects hardly detectable in ground-based imaging surveys.

Dwarf elliptical thus represent a heterogeneous class of galaxies. Most probably several different mechanisms, including environmental effects as galaxy harassment and ram pressure stripping, are involved in the creation of the overall population of dEs.

Ultracompact dwarf galaxies (UCDs) have properties between dwarf ellipticals and globular clusters. They were first discovered in the Fornax and Virgo clusters (Hilker et al. 1999; Drinkwater et al. 2000; Haşegan et al. 2005). They are also found around giant galaxies in nearby groups. Ultracompact dwarfs are characterized by predominantly old stellar populations (≥ 8 Gy, e.g., Chilingarian et al. 2011), small sizes (half-light radii of $10 \leq r_h \leq 100$ pc), and dynamical masses of $2 \times 10^6 \leq M \leq 10^8 M_\odot$ (Hilker et al. 2007; Mieske et al. 2008). As dEs, ultracompact dwarfs represent a heterogeneous class of objects (Mieske et al. 2006). They might be (i) very massive globular clusters, (ii) tidally stripped nucleated dEs (Bekki et al. 2001), or (iii) end products of small-scale primordial density fluctuations in dense environments (Phillipps et al. 2001). It is suggested that the most massive ultracompact dwarfs are remnants of more extended galaxies, whereas the less massive ones represent a transition objects toward the regime of ordinary globular clusters (Chilingarian et al. 2011).

If tidal stripping acts on massive progenitors, one would expect the remnants to be larger and more luminous than UCDs. An example of such an object is M 32, a *compact elliptical* (cE) satellite of the Andromeda Galaxy. It has a luminosity comparable to typical dE in clusters but

10 times smaller half-light radius, therefore 1,000 times higher stellar density per unit of volume. For several decades cE galaxies were considered unique since only three of them including M 32 were known and several dedicated searches failed to detect any. Therefore, even solid arguments for M 32 to be a heavily tidally stripped lenticular galaxy (Graham 2002) did not allow to consider tidal stripping an important channel of galaxy evolution because of the lack of examples. The situation might change with the discovery of a population of 21 cE galaxies in nearby galaxy clusters by Chilingarian et al. (2009). These authors showed that the properties of the cE galaxies can be reproduced by numerical simulations of tidal stripping.

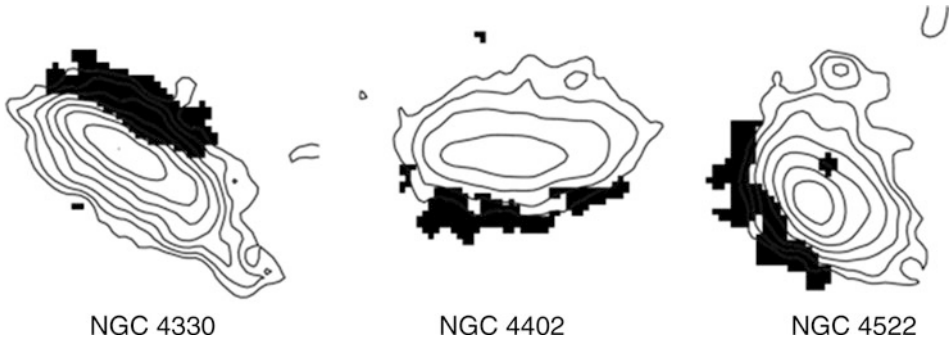
8 Resolved Multiwavelength Interaction Diagnostics

Can we catch a galaxy with an ongoing environmental interaction? To do so, imaging observations with a spatial resolution of ~ 1 kpc are necessary. With multiwavelength imaging observations, the reaction of the multiphase interstellar medium and star formation to these interactions can be studied in detail. Deep optical imaging reveals perturbations of the galaxy's stellar content due to tidal interactions. The comparison between optical and interferometric HI observations can discriminate between tidal and hydrodynamic interactions. Since ram pressure only affects the gas, a symmetric stellar disk with a truncated gas disk within the optical radius and a one-sided gas tail in a cluster galaxy are signs of ongoing ram pressure stripping (e.g., Chung et al. 2007). In rare cases, extraplanar molecular gas traced by its CO emission can also be found (Combes et al. 1988; Vollmer et al. 2005b, 2006). Perturbed and extraplanar star formation distributions are observed in $H\alpha$ (e.g., Koopmann and Kenney 2004b) or UV (e.g., Abramson et al. 2011). Sometimes the radio continuum halo can be compressed on the side where ram pressure is acting (Gavazzi et al. 1995; Crowl et al. 2005). In rare cases, an extended one-sided X-ray tail is detected (e.g., Sun et al. 2006).

Relatively new diagnostic tools are the polarized radio continuum and radio/FIR distributions of cluster spiral galaxies.

Under the assumption of a constant FIR-radio correlation within normal galaxies, Murphy et al. (2009) used Spitzer infrared data to create model radio maps, which were compared to observed radio images. These authors found that galaxies, which are affected by ram pressure stripping, have enhanced global radio fluxes with respect to the FIR. These galaxies contain regions along their outer edges where the observed radio surface brightness is significantly below the model expectation (see Fig. 5-8). The radio-deficient regions are located in the direction of the ram pressure wind and often show an enhanced polarized radio continuum emission (see Fig. 5-9 for NGC 4522).

Polarized radio continuum emission is due to relativistic electrons with density n_e gyrating around the regularly oriented, large-scale magnetic field B : $S_{\text{PI}} \propto n_e B^2$. The polarized radio continuum emission is enhanced in regions where shear and compression of the regular or random magnetic field component parallel to the sky plane occur. From spectroscopic observations, noncircular motions of the order of ~ 10 km s^{-1} induced by an interaction can be determined by a detailed analysis of a galaxy's velocity field (e.g., Schoenmakers et al. 1997). On the other hand, the distribution of polarized radio continuum emission represents a very sensitive tool for uncovering the transverse motions of the ISM (Beck 2005) even in the case of unfavorable inclinations (close to face-on). Therefore, the information contained in polarized radio continuum emission is complementary to that of $H\alpha$, CO, and HI observations. The total



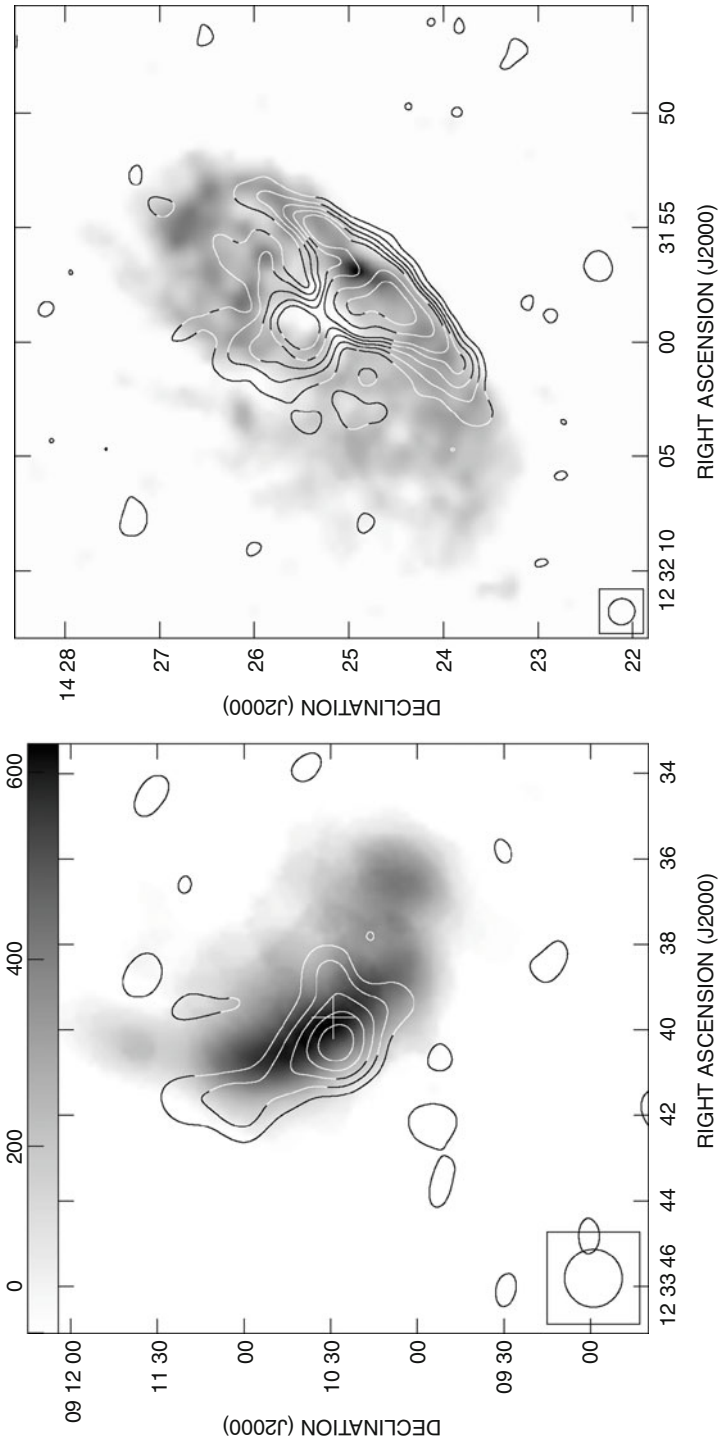
■ Fig. 5-8

Radio-deficient regions of the Virgo cluster spiral galaxies NGC 4330, NGC 4402, and NGC 4522 with radio continuum contours (From Murphy et al. 2009)

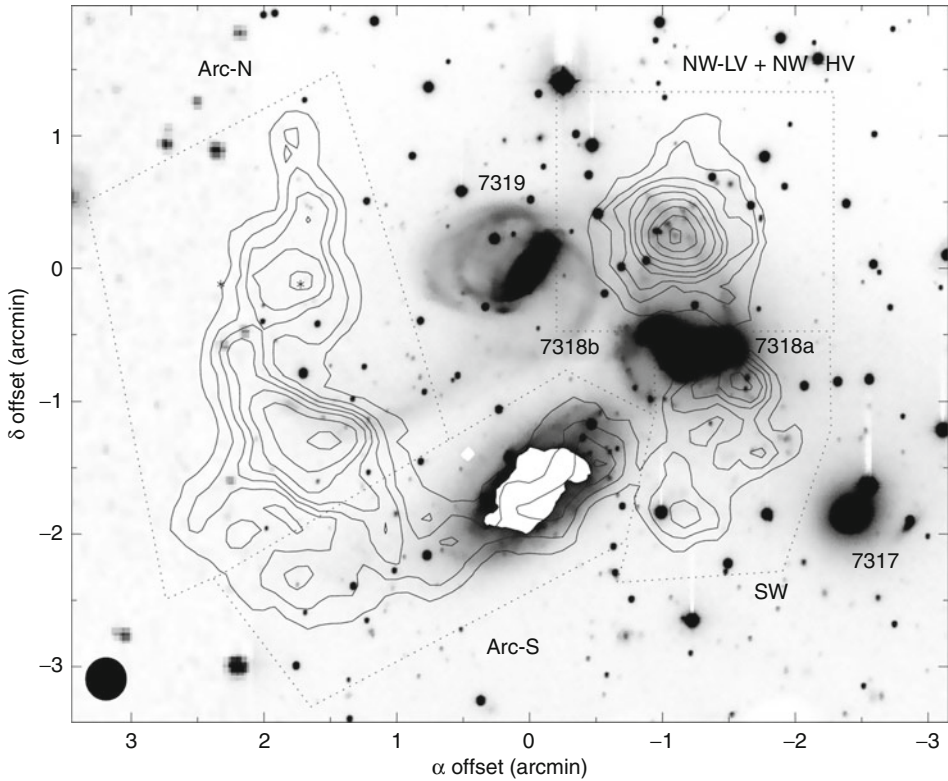
radio continuum emission is sensitive to the turbulent small-scale magnetic field, which is usually a factor of 2–5 larger than the regular large-scale magnetic field in spiral arms and 1–2 times larger in the interarm regions at a typical resolution of a few 100 pc (Beck 2001). Whenever there is enhanced turbulence due to an enhanced star formation efficiency, the large-scale magnetic field is diminished. The polarized radio continuum emission has to be observed at a frequency that is high enough to avoid significant Faraday rotation (typically >2 GHz). In a pioneering work, Vollmer et al. (2007) presented 6 cm polarized radio continuum emission of 8 Virgo spiral galaxies. All galaxies show strongly asymmetric distributions of polarized intensity with elongated ridges located in the outer galactic disk. These features are not found in existing observations of polarized radio continuum emission of field spiral galaxies, where the distribution of 6 cm polarized intensity is generally relatively symmetric and strongest in the interarm regions. Once an asymmetric distribution of polarized radio continuum emission is detected, one has to discriminate between shear or compression motions as its cause. In the case of ram pressure compression, one expects an H I gas tail at the opposite side of the compression region (e.g., Vollmer et al. 2004b; ► Fig. 5-9). Tidal interactions can lead to compression and shear motions (Soida et al. 2006).

8.1 Environmental Effects in Nearby Galaxy Groups

In galaxy groups, encounters between two galaxies are the most important environmental effect. Relative velocities between galaxies are small, and for small impact parameters, tidal fields produce important distortions of the stellar and gaseous content of the galaxies. Since galaxy density is highest in compact groups, galaxy encounters occur frequently in this environment. One of the best studied compact group is Stephan's Quintet which is made of four group galaxies and one foreground object. A fifth galaxy, situated $\sim 4'$ to the east, is also dynamically associated to the group. The group has experienced a violent dynamical history with numerous interactions between the different members during the past Gyr. As a result of these interactions, two tidal arms, a faint older one and a brighter young one stemming from NGC 7319, have been created toward the eastern side of the group (Sulentic et al. 2001). The other group spiral galaxies show important tidal perturbations. Because of these interactions, most of the gas is found



■ Fig. 5-9 6-cm polarized radio continuum emission (contours) on the HI distribution (greyscale) of the ram pressure stripped Virgo spiral galaxies NGC 4522 (left; from Vollmer et al. 2004b) and NGC 4501 (right; from Vollmer et al. 2010). The regions of gas compression visible in the polarized radio continuum are on the opposite side of the extraplanar HI or HI extensions



■ Fig. 5-10

Stephan's Quintet. Map of the total HI column density distribution (contours) superposed on the R-band image (from Williams et al. 2002). The galaxy with the white area (NGC 7320) is in the foreground. The HI projected onto this galaxy actually belongs to the group

in a highly disturbed intragroup medium (☉ Fig. 5-10; Williams et al. 2002). The last and presumably ongoing event involves the collision of the gas-rich spiral NGC 7318b with the debris field produced by past interactions.

Due to the dense environment, galaxy and group evolution is accelerated in compact groups. In Stephan's Quintet, we can directly observe galaxy transformation via multiple gravitational encounters. In this way, gas and stars are loosened and eventually removed from the parent galactic disks. The fraction of the diffuse light from tidally stripped stars to the total light from the group can be up to ~50% in compact groups (da Rocha and Mendes de Oliveira 2005). Galaxy mergers lead to lenticular or elliptical galaxies. Indeed, there are compact groups whose galaxy populations are dominated by early-type galaxies (e.g., Huchtmeier 1997). Since gas disks of normal spiral galaxies are more extended than stellar disks, the amount of expelled gas is larger than that of stars. This gas then forms an intragroup medium. It is expected to be heated through evaporation in a previously existing intragroup medium or through large-scale shocks from freshly accreting material falling into the galaxy group.

To investigate the importance of ram pressure stripping in compact groups, Rasmussen et al. (2008) analyzed the diffuse X-ray emission of 8 HI-deficient Hickson compact groups.

If ram pressure stripping were the dominant cause of HI removal, one would expect an important intragroup medium traced by X-ray emission in these groups. Their finding that the most HI-deficient groups do not show a detectable hot intragroup medium suggests that tidal interactions are the most likely cause of gas removal. This is consistent with the absence of a correlation between the fraction of HI-deficient galaxies in a group and the X-ray luminosity in the sample of Kilborn et al. (2009). On the other hand, HI imaging of spiral galaxies in X-ray bright groups (Sengupta et al. 2007) revealed disturbed morphologies and truncated gas disks compared to field spirals. The observed gas disk truncation might be an indication that ram pressure stripping plays a role in groups with a prominent intragroup medium.

Thus, for the overall statistics tidal interaction dominates and ram pressure seems to play a minor role in the evolution of group spiral galaxies. However, in X-ray bright groups, it may represent an additional cause for the observed HI deficiency. Most probably, the ISM has to be loosened tidally to be stripped efficiently by ram pressure. In rare cases, arriving spiral galaxies can undergo important ram pressure if the intragroup gas is still in the form of relatively dense tidal tails of atomic gas from a previous galaxy–galaxy encounter. As an example, Clemens et al. (2000) presented the case of ram-pressure stripping by a gaseous tidal tail in the interacting pair of galaxies NGC 4490/4485.

8.2 Environmental Effects in Nearby Galaxy Clusters

Multiwavelength imaging observations of cluster galaxies give insights when and where in the cluster a galaxy experiences an environmental interaction and how its different components are affected by this interaction. In the following, we will have a look at five close galaxy clusters: Coma, Norma, Abell 1367, Virgo, and Fornax. The five clusters represent quite different environments. The Coma, Norma, and Abell 1367 clusters are more massive than the Virgo and Fornax clusters. Whereas the Norma and Virgo clusters are dynamically active with galaxy subgroups or clusters falling onto and merging with the main cluster, Coma and Fornax are more dynamically quiescent, i.e., their galaxy accretion rates are much lower than those of Norma, Abell 1367, and Virgo. However, even in the more quiet systems galaxies and galaxy groups are still falling into the main cluster. The fraction of HI-deficient galaxies is large in Coma, Virgo, and Norma and intermediate in Abell 1367. Galaxies in the Fornax cluster do not show signs of strong HI deficiency (Horellou et al. 1995). In the following, the properties of these clusters sorted by velocity dispersion are presented.

1. The *Coma cluster* is a massive relaxed cluster with a mass of $\sim 5 \times 10^{14} M_{\odot}$ within 1 Mpc and galaxy velocity dispersion of 950 km s^{-1} . It is the richest nearby (~ 90 Mpc) cluster and represents the end product of an ancient merger of two clusters. The dominating two central elliptical galaxies, NGC 4874 and NGC 4889, are reminiscent of this merger. The Coma cluster is spiral-poor which is typical for rich clusters. Despite the symmetric galaxy distribution, a galaxy group in the southwest of Coma, associated with the giant elliptical galaxy NGC 4839, has probably passed the cluster core in the recent past. The cluster is X-ray luminous, has a symmetric main component with an extended intracluster medium distribution, and has some substructure related to galaxy groups (Briel et al. 1992). For a review on the Coma cluster, see Biviano (1998).
2. The *Norma cluster* (Abell 3627) is the nearest (~ 65 Mpc) rich, massive cluster of galaxies (Kraan-Korteweg et al. 1996; Woudt 1998), with properties comparable to the Coma cluster

(Mazure et al. 1998). It has remained relatively unexplored in comparison to its well-known counterpart, mainly because of its location at low galactic latitudes in the southern zone of avoidance (ZOA) where dust extinction and star crowding dilute its appearance. The dynamical mass of the Norma cluster is $\sim 10^{15} M_{\odot}$ within its Abell radius of 2 Mpc. The galaxy velocity dispersion is 925 km s^{-1} (Woudt et al. 2008). The spiral/irregular galaxies reveal a large amount of substructure. The X-ray emission distribution is not spherically symmetric and shows indications of an ongoing cluster merger (Böhringer et al. 1996).

3. *Abell 1367* forms together with the Coma cluster the Coma-Abell 1367 supercluster at a distance of ~ 90 Mpc. Its velocity dispersion is 880 km s^{-1} (Moss et al. 1998). The cluster is a rather unusual example of a rich cluster with a comparatively high fraction of spiral galaxies. It has been identified as having significant optical and X-ray substructure (Grebenev et al. 1995). The X-ray emission is elongated along a southeast-northwest axis and contains small, localized clumps. This is interpreted as a merger of two subclusters (Donnelly et al. 1998). The high spiral fraction and a relatively cool intracluster medium temperature (Donnelly et al. 1998) are typical of what is expected for a dynamically young system.
4. The *Virgo cluster* is less massive ($\sim 2 \times 10^{14} M_{\odot}$ within 1.5 Mpc) and has a galaxy velocity dispersion of $\sim 600 \text{ km s}^{-1}$. It represents the nearest cluster (17 Mpc) in the northern hemisphere. The Virgo cluster is spiral-rich and has a lot of substructure (see, e.g., Schindler et al. 1999). Different galaxy groups can still be distinguished spatially and kinematically from the main cluster. Virgo is thus said to be dynamically young. Its X-ray luminosity is ~ 6 times smaller than that of the Coma cluster. X-ray emission can be associated to the main cluster, where it is strongly peaked on the central elliptical galaxy M 87, and several substructures (Böhringer et al. 1994).
5. After Virgo, the largest concentration of galaxies within 20 Mpc is the *Fornax cluster*. Its spiral-rich galaxy distribution has a more regular shape than that of the Virgo cluster, indicating a more dynamically evolved state. Fornax is also considerably smaller and denser than Virgo, with a core radius $\sim 40\%$ that of Virgo and a central density twice as large. The total mass of Fornax is $0.7\text{--}2 \times 10^{14} M_{\odot}$ within ~ 1 Mpc (Drinkwater et al. 2001; Dunn and Jerjen 2006), its velocity dispersion 380 km s^{-1} (Drinkwater et al. 2001). The X-ray emission shows an asymmetric spatial distribution, and the central elliptical galaxy, NGC 1399, is offset from the center (Paolillo et al. 2002), which may be related to large-scale dynamical evolution such as infall motions of galaxies into the cluster (Dunn and Jerjen 2006).

In a cosmological context, galaxies assemble into small groups which then merge forming large groups or small clusters like Fornax. A central cluster is growing with the accretion of groups and small clusters (Virgo). When two big clusters merge, they have the appearance of Abell 1367 or the Norma cluster. Without further accretion, the cluster virializes and becomes spherical (Coma). Galaxy clusters can be classified according to their degree of relaxation. Non-relaxed clusters have an irregular overall shape, are spiral-rich, and have a low X-ray luminosity. On the other hand, relaxed clusters are spherical, rich of early-type galaxies, and have a high X-ray luminosity. However, not all clusters follow these rules. Each cluster is different and has its own personality according to its assembling history. This cosmological scenario is further discussed in [Sect. 10](#).

In the next section, we will have a close look at resolved multiwavelength observations of cluster galaxies. Early-type cluster galaxies have a corona of abundant hot gas (several 10^6 K), which is in hydrostatic equilibrium with the galaxy's gravitational potential and emits in X-rays. In addition, small amount of cold gas $\sim 10^8 M_{\odot}$ are often found in the galaxy cores. The ISM of

late-type galaxies has a multiphase structure with a dominant neutral warm and cold phase as described in [Sect. 5](#). It is confined within the galactic disk and supported by rotation. Dwarf spiral and irregular galaxies possess a neutral warm/cold ISM which is either supported by rotation and velocity dispersion, respectively. Due to the shallow potential well of these galaxies, their gas content can be removed easily by environmental interactions. Because of these differences, early-type, late-type, and dwarf galaxies will be discussed separately.

8.2.1 Early Type Galaxies

In early-type cluster galaxies, the hot corona is exposed to the intracluster medium. Environmental effects are thus detectable in X-ray emission. The signpost of ram pressure compression is a sharp edge on one side of the galaxy. The X-ray surface brightness drops by an order of magnitude over the edge. These “cold fronts” are contact discontinuities, in which a sharp drop in surface brightness (gas density) is accompanied by a corresponding rise in gas temperature. This is characteristic for the motion of a spheroid through a uniform gas and is consistent with a jumplike density discontinuity at the boundary in the direction of the galaxy’s motion within the intracluster medium. The sharpness of the edge is a strong function of the inclination angle between the galaxy’s 3D velocity vector and the plane of the sky. The edge is most prominent if the galaxy has a negligible radial velocity with respect to the surrounding intracluster medium. Sometimes, an X-ray low surface brightness tail can be found at the opposite side of the sharp edge (e.g., Machacek et al. 2006).

X-ray spectra yield information on the density, temperature, and metallicity of the interstellar medium of the elliptical galaxy and the intracluster medium. The ISM density and temperature are typically $n_{\text{ISM}} \sim$ a few 10^{-3} cm^{-3} and $T \sim 0.5 \text{ keV} = 6 \times 10^6 \text{ K}$ with an about solar metallicity. The density and metallicity of the intracluster medium are smaller, and its temperature is higher ($T_{\text{ICM}} \geq 1.5 \text{ keV} \sim 2 \times 10^7 \text{ K}$). The pressure jump can be used to determine the Mach number M_1 and thus the velocity with which the galaxy moves through the intracluster medium (Landau and Lifshitz 1959). For a subsonic motion ($M_1 \leq 1$):

$$\frac{p_0}{p_1} = \left(1 + \frac{(\gamma - 1)}{2} M_1^2 \right)^{(\gamma/\gamma-1)}, \quad (5.9)$$

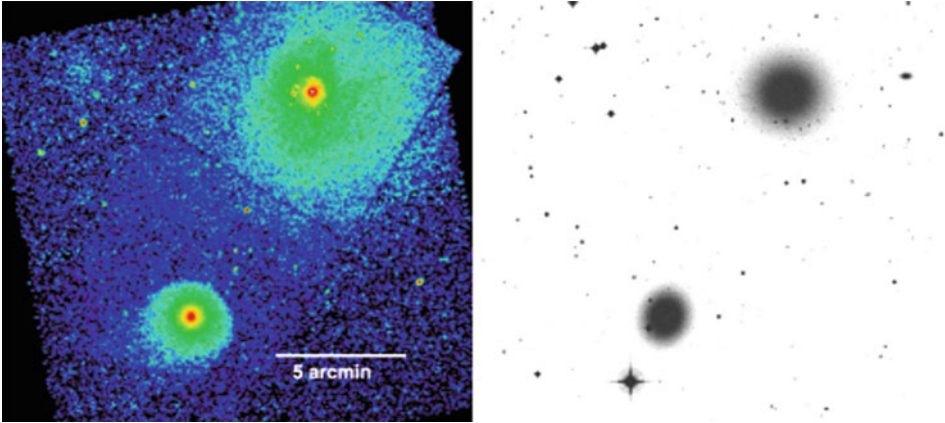
for supersonic motions ($M_1 > 1$):

$$\frac{p_0}{p_1} = \left(\frac{\gamma + 1}{2} \right)^{(\gamma+1)/(\gamma-1)} M_1^2 \left(\gamma - \frac{\gamma - 1}{2M_1^2} \right)^{-1/(\gamma-1)}, \quad (5.10)$$

where $\gamma = 5/3$ is the adiabatic index for a monoatomic ideal gas and p_0/p_1 the gas pressure in the ISM and the intracluster medium, respectively. Together with the observed radial velocity of the galaxy, the transverse velocity in the plane of the sky and the inclination angle between the galaxy’s 3D velocity and the plane of the sky can be determined. The latter has to be consistent with the observed X-ray morphology.

With this method, Machacek et al. (2005) derived a pressure jump of $p_0/p_1 \sim 2$ implying a Mach number of $M_1 \sim 1$ for the elliptical galaxy NGC 1404 in the Fornax cluster ([Fig. 5-11](#)). This galaxy is approaching the dominant elliptical galaxy of the Fornax cluster, NGC 1399, and undergoes significant ram pressure by the Fornax cluster intracluster medium.

Another example of a cluster elliptical galaxy undergoing active ram pressure is NGC 4552 (M 89) in the Virgo cluster. This galaxy is located at a projected distance of $72' = 360 \text{ kpc}$ east



■ Fig. 5-11
Chandra ACIS X-ray (left) and DSS (right) images of NGC 1404 (southeast, lower left) and NGC 1399 (northwest, upper right) galaxies in the Fornax cluster (From Machacek et al. 2005)

of M 87, the central elliptical galaxy of the Virgo cluster. NGC 4552 has an extended (~ 10 kpc) X-ray low surface brightness tail (Machacek et al. 2006). The properties of the X-ray tail are consistent with it being composed primarily of ram pressure stripped galaxy gas. The tail is denser and cooler than the Virgo intracluster medium. On the opposite side, a classical cold front is detected. Galaxy gas inside the leading edge is cool ($kT = 0.43$ keV) compared to the surrounding 2.2-keV Virgo intracluster medium. The pressure ratio of ~ 7 across the leading edge of the ram pressure interaction corresponds to a Mach number of ~ 2 . Two horns of emission extending 3–4 kpc to either side of the edge are composed of gas in the process of being stripped from the galaxy due to the onset of Kelvin-Helmholtz instabilities. This galaxy thus also undergoes turbulent viscous stripping (see ► Sect. 3.2).

The same overall X-ray morphology is found in another massive Virgo elliptical galaxy, NGC 4472 (M 49; Biller et al. 2004), which is located at a projected distance of 1.3 Mpc south of M 87. A tail-like structure in the X-ray emitting gas extends $\sim 8' = 36$ kpc to the southwest of the galaxy core. The northeastern edge in the X-ray emission distribution is most probably the result of ram pressure compression as NGC 4472 falls toward the center of the Virgo cluster.

The most enigmatic elliptical galaxy in the Virgo cluster is M 86. The second brightest Virgo elliptical galaxy is located at a projected distance of only 350 kpc from M 87 and has a high radial velocity with respect to the Virgo cluster mean ($\sim 1,000$ km s $^{-1}$). It might be located as far as 1 Mpc behind M 87 (Mei et al. 2007). An X-ray study of M 86 with Einstein (Forman et al. 1979) revealed a peak of emission centered on M 86 and a plume extending northwest of the galaxy. Subsequent observations showed substructure in the M 86's X-ray halo. Finoguenov et al. (2004a) revealed a cold front in the southwest of the galaxy core which is most probably due to ram pressure compression. They ascribed the huge X-ray plume to a gravitational interaction. This scenario has gained support by the detection of faint H α emission connecting the perturbed spiral galaxy NGC 4438 to M 86 (► Fig. 5-17; Kenney et al. 2008). On the other hand, Randall et al. (2008) suggested that the X-ray plume is due to ram pressure stripping.

8.2.2 Late Type Galaxies


Tidal interactions lead to asymmetries in the stellar distribution of the galactic disk observable in the NIR, optical, and UV. The signposts of ram pressure stripping are (i) gas disks which are truncated inside the optical radius, (ii) one-sided HI tails together with a symmetric old stellar disk, and (iii) radio-deficient regions and/or asymmetric ridges of polarized radio continuum emission located in the outer-disk opposite to the gas tail (► Fig. 5-9). One-sided tails of warm or hot gas observable in H α and X-rays are much rarer than tails of atomic gas. Radio continuum tails are the exception. A significant fraction of perturbed cluster galaxies undergo a tidal interaction and ram pressure stripping at the same time. In the following, an inventory of environmentally affected disk galaxies in the different nearby clusters is presented.

Coma Cluster

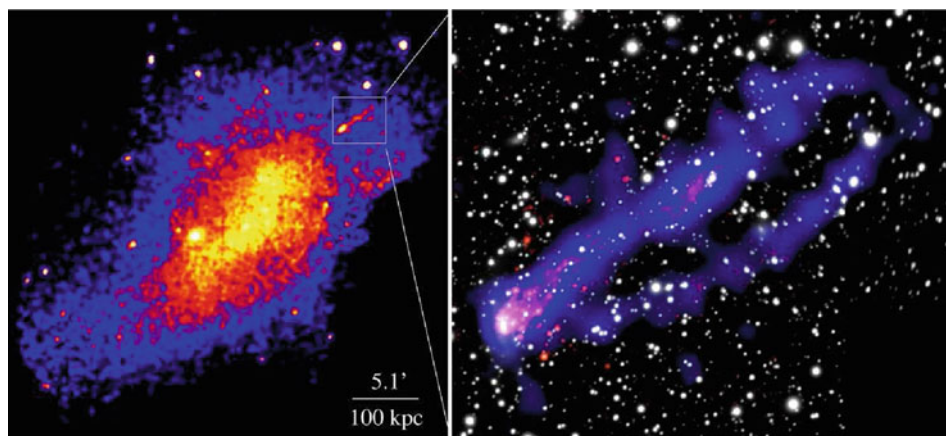
Bravo-Alfaro et al. (2000) imaged the 19 brightest spiral galaxies in the *Coma cluster* in the HI line (► Fig. 5-12). The galaxies, which are located at projected distances smaller than $d = 0.6$ Mpc, show truncated gas disks with pronounced asymmetries in their atomic gas distributions and/or shifts between the optical and the HI positions. Twelve spiral galaxies were not detected with typical upper HI mass limits of $10^8 M_{\odot}$. Seven of the twelve non-detections are located in the central region of Coma ($d < 0.6$ Mpc). In addition to HI asymmetries, UV and H α asymmetries seem to be a common property of ram pressure stripped Coma cluster galaxies. Whereas the UV emission only traces young massive stars, the H α emission can also provide from ionized dense gas. Yagi et al. (2010) found extended H α clouds associated with 14 Coma cluster galaxies obtained from deep narrow-band imaging observations with the Subaru Telescope. The parent galaxies are blue and distributed farther than 0.2 Mpc from the peak of the X-ray emission of the cluster. Smith et al. (2010) found tails or trails of UV-bright debris in 13 star-forming Coma cluster galaxies, which they interpreted as young stars formed within gas stripped by ram pressure from the intracluster medium. Within 1 Mpc projected distance from the cluster center, about 30% of blue galaxies show UV trails. These trails are predominantly oriented away from the cluster center, indicating that the galaxies are falling into the cluster for the first time, along radial orbits.


One of the Coma spiral galaxies barely detected in HI is NGC 4848 (CGCG 160-055 on ► Fig. 5-12). This highly inclined spiral galaxy is located on the outermost X-ray contour northwest of the cluster center. The atomic gas is displaced to the northwest with respect to the optical disk. Its molecular gas distribution is also asymmetric with an off-center secondary maximum coincident with the inner part of the displaced atomic gas (Vollmer et al. 2001b). The H α emission shows a double line in this conspicuous region. One line is due to galaxy rotation, the other line is most probably gas accelerated by ram pressure. Furthermore, an X-ray tail is detected to the northwest which is more extended than the HI emission (Finoguenov et al. 2004b). An estimation of the stripping radius (► 5.2) based on the intracluster medium density at the projected distance of NGC 4848 given by Briel et al. (1992) and a galaxy velocity of $2,000 \text{ km s}^{-1}$ yields a stripping radius twice as large as the edge of the gas and star formation. Thus, either the galaxy already had its closest approach to the cluster center and is now leaving the cluster core as proposed by Vollmer et al. (2001a), or the intracluster medium has an overdensity or moves in the direction opposite to that of the galaxy's motion (see ► Sect. 9).

Norma Cluster

The detection of long one-sided X-ray tails is very rare compared to H α detections. The most spectacular example is that of the late-type galaxy ESO 137-001 (Sun et al. 2006, 2007, 2010;  Fig. 5-13), which is most probably stripped nearly face-on. The projected distance from the cluster's X-ray peak of this blue emission-line galaxy is only 180 kpc. About 80% of the galaxy's total X-ray emission corresponding to a gas mass of $\sim 10^9 M_{\odot}$ is found behind the galactic halo. The X-ray tail consists of two components: a straight and thin (~ 8 kpc) main tail with a size of ~ 80 kpc and a secondary fainter and curved X-ray tail. The main tail is brightest in the middle and near the galactic disk. The gas temperature in the tail is constant ($kT \sim 0.8$ keV) and significantly lower than that of the surrounding intracluster medium ($kT \sim 6$ keV). The soft X-ray emission of the tail comes from the mixing of cold ISM with the hot intracluster medium. Diffuse H α is associated with the X-ray tail. Close to the galactic disk (< 20 kpc), Sivanandam et al. (2010) detected $2.5 \times 10^7 M_{\odot}$ of shocked, warm molecular hydrogen. An important number of HII regions are detected near or close to the X-ray tail up to a projected distance of ~ 40 kpc from the galactic disk. Thus, star formation proceeds in situ in the stripped material. The imprint of galactic rotation is still present in the velocity map of these HII regions. It seems that the gas turbulence in the stripped gas tail did not greatly enhance the velocities of the extraplanar HII regions.

A second 40-kpc-long X-ray tail has been detected behind another late-type galaxy, ESO 137-002 (Sun et al. 2010). Signature of gas stripping were also found in the H α data, with a sharp H α edge and an H α tail extending to at least 20 kpc from the galactic nucleus. No HII regions are found in this tail. The X-ray morphology points to a more edge-on stripping.



 Fig. 5-13

Left: XMM-Newton 0.5–2 keV mosaic of the galaxy cluster Abell 3627. The main tail of ESO 137-001 is significant in the XMM-Newton image. *Right:* the composite X-ray/optical image of ESO 137-001's tail. The Chandra 0.6–2 keV image is in blue, while the net H α emission is in red and the stellar image in white (From Sun et al. 2010)

Abell 1367

The only disk galaxies with a long one-sided radio continuum tail are CGCG 97-073 and CGCG 97 079 in the *galaxy cluster Abell 1367* (Gavazzi et al. 1995). Faint H α emission is associated with these tails. The sizes of the tails are 50–75 kpc. The H I distributions of the two galaxies are offset from the galaxy centers in the direction coincident with the radio continuum tails (Dickey and Gavazzi 1991). All observations are consistent with a scenario where both galaxies are undergoing ram pressure stripping. The two galaxies are located at the periphery of a sub-cluster merging with the main cluster. The X-ray morphology of Abell 1367 is similar to that of the Norma cluster. The intracluster medium associated with the subcluster is significantly hotter than that of the main cluster. Another galaxy in this region, UGC 6697, has an X-ray tail and a sharp edge in the X-ray distribution at the opposite side (Sun and Vikhlinin 2005). Since Gavazzi et al. (2001) proposed a scenario where UGC 6697 is composed of two interacting galaxies and the system shows a prominent stellar tail, a tidal interaction and ram pressure stripping most probably act together.

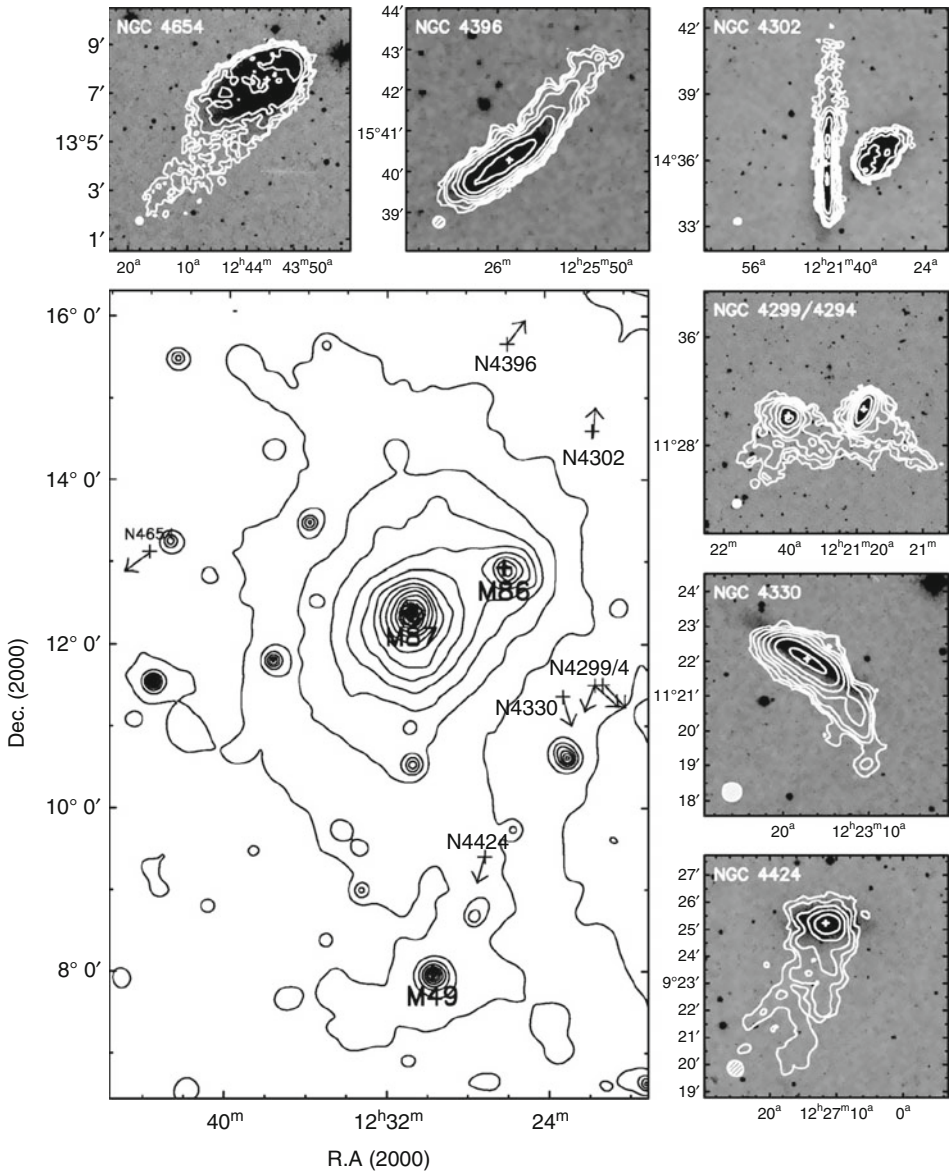
Virgo Cluster

In the H I imaging survey of Virgo galaxies (VIVA: VLA Imaging of Virgo galaxies in Atomic gas), Chung et al. (2007) found seven spiral galaxies with long H I tails (☛ Fig. 5-14). These tail galaxies have the following properties in common in the H I morphology: (i) the H I is extended well beyond the optical disk only on one side; (ii) the tails differ from tidal bridges; i.e., there is no optical counterpart at the tip of the tail down to $r \sim 26$ mag arcsec $^{-2}$ in the Sloan Digital Sky Survey (SDSS) images; and (iii) the projected length of the gas tail is larger than half of the symmetric part in H I. These galaxies are found in intermediate- to low-density regions (0.6–1 Mpc in projection from M 87). The tails are all pointing roughly away from M 87. At least three systems show H I truncation to within the stellar disk, providing evidence of a gas–gas interaction. A comparison between the estimated (based on ☛ 5.2) and observed stripping radii suggests that simple ram pressure stripping could have indeed formed the tails in all but two cases. One of these cases is NGC 4654 where ram pressure stripping is facilitated by a tidal interaction (see below). The H I observations of this spiral galaxy sample represents evidence that ram pressure stripping already begins to affect spiral galaxies around the cluster virial radius. At least 25% of the large spiral galaxies in the region between 0.6 and 1 Mpc from the Virgo cluster center seem to be recent arrivals being stripped of gas.

There are four cases of a mixed interaction, i.e., the combination between a tidal interaction and ram pressure stripping, in the Virgo cluster: NGC 4424, NGC 4654, NGC 4254, and NGC 4438. In the following their properties are described in detail. Other galaxies affected by ram pressure stripping are described in ☛ Sect. 8.3.

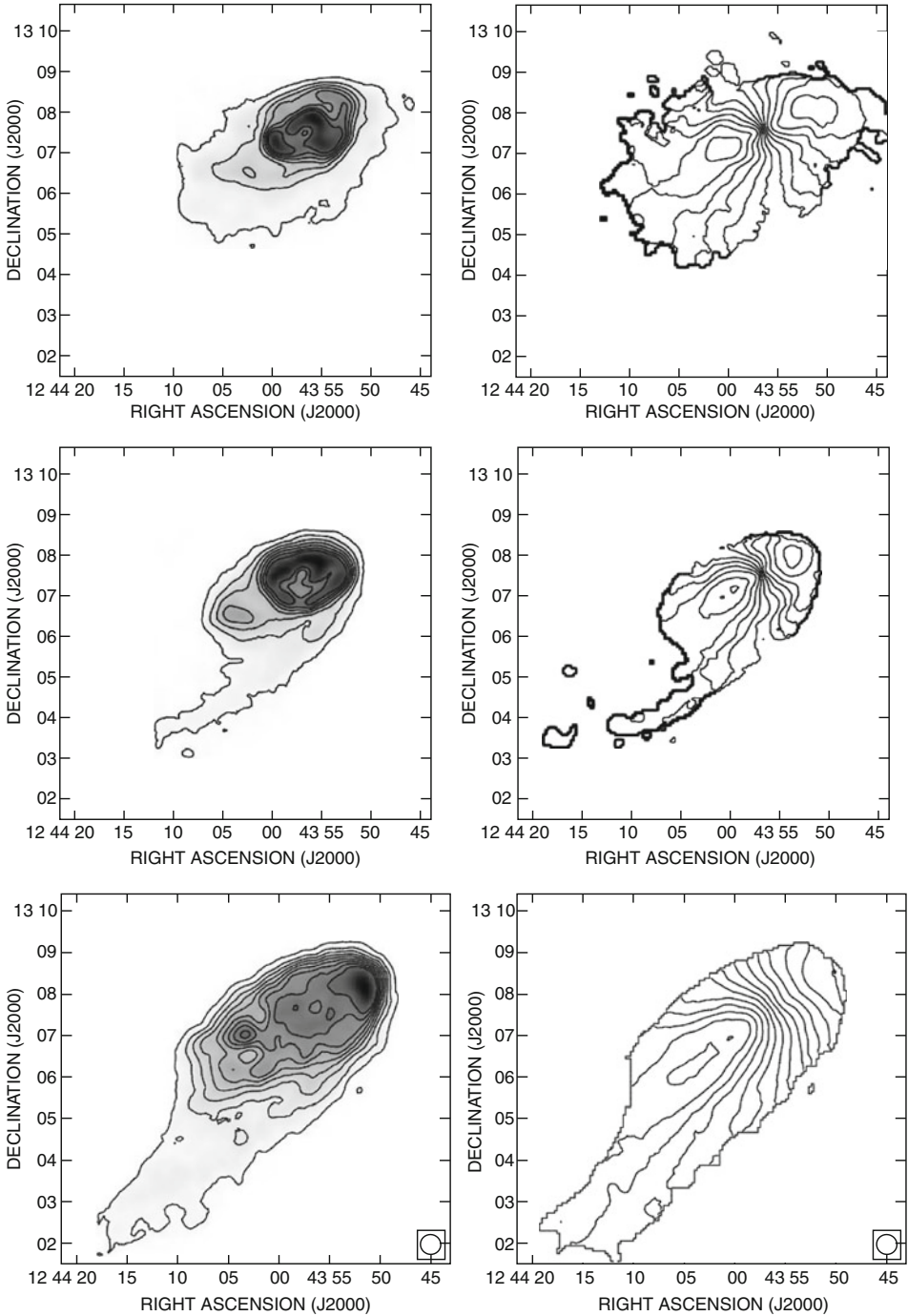
The broadband optical appearance of NGC 4424 is peculiar, with shell-like features and banana-shaped isophotes, suggesting a major gravitational disturbance or a merger (Kenney et al. 1996). This galaxy has extremely modest stellar rotation velocities (~ 30 km s $^{-1}$), and stars are supported by random motions as far out as it can be measured (1.4 kpc). The ionized gas kinematics in the core are disturbed and possibly counterrotating. Cort ese et al. (2006) suggested that the peculiarities of NGC 4424 are the result of an intermediate-mass merger plus ram pressure stripping which created the long one-sided H I tail detected by Chung et al. (2007).

The spiral galaxy NGC 4654 is located at a projected distance of $3.4^\circ \sim 1$ Mpc from the cluster center (☛ Fig. 5-5). It is one of the galaxies with a long one-sided H I tail of Chung et al. (2007). The velocity field of the tail does not show rotation (☛ Fig. 5-15). This galaxy



■ Fig. 5-14

In the main large panel, the locations of the H I tail galaxies are shown as the crosses on the X-ray background of the Virgo region. The directions of the tails are indicated with the arrows. The second tail of NGC 4299 (east tail) is shown in *light gray*. In the six smaller panels on the top and on the right, we show zoomed views of individual galaxies. The H I contours (*white*) are shown overlaid on the Digitized Sky Survey (DSS) image in gray scale (From Chung et al. 2007)



■ Fig. 5-15

The Virgo cluster spiral NGC 4654. *Left:* H I distribution, *right:* H I velocity field. *Upper panels:* gravitational interaction model, *middle panels:* gravitation interaction + ram pressure stripping model, *lower panels:* H I observations (From Vollmer 2003)

also shows an asymmetric stellar distribution. Numerical simulations using ram pressure as the only perturbation can produce a tail structure of the gas content but cannot account for its kinematical structure. Simulations using a gravitational interaction with the companion galaxy NGC 4639 can account for the asymmetric stellar distribution of NGC 4654 but cannot reproduce the observed extended gas tail. Only a mixed interaction, gravitational and ram pressure, can reproduce all observed properties of NGC 4654 (Vollmer 2003; [Fig. 5-15](#)). The tidal interaction loosened the gas from the galaxy's gravitational potential. Only a small amount of ram pressure, about 1/4 of the ram pressure estimated using ([Fig. 5.2](#)), is necessary to produce the observed H I tail.

The spiral galaxy NGC 4254 is located at the same projected distance as NGC 4654 (~1 Mpc) on the other side of the Virgo cluster. The spiral structure of NGC 4254 shows an important $m = 1$ mode, giving it a one-armed appearance. Deep VLA H I observations (Phookun et al. 1993) revealed, in addition to the galactic H I disk component, H I clouds superposed on and beyond the gas disk with velocities that do not follow the disk rotation pattern. Very low surface density atomic gas is found up to $\sim 6'$ (~ 30 kpc) to the north-west of the galaxy center. Subsequent WSRT (Minchin et al. 2007) and Arecibo (Haynes et al. 2008) H I observations revealed the longest low surface density gas tail ever observed with a length of ~ 250 kpc ([Fig. 5-16](#)). This tail structure could be reproduced by a rapid ($\sim 1,000$ km s $^{-1}$) and close (~ 60 kpc) flyby of a massive galaxy (1.5 times the mass of NGC 4254) by Duc and Bournaud (2008). The smooth velocity field with a reversal of the gradient in the middle of the tail is a natural result of the dynamical model ([Fig. 5-16](#)). As in NGC 4654, ram pressure might act on the gas loosened by the gravitational interaction (Vollmer et al. 2005a; Kantharia et al. 2008).

NGC 4438 has the most spectacular tidal tails in the Virgo cluster ([Fig. 5-1](#)). It is located at a projected distance of only $1^\circ = 300$ kpc from the cluster center (M 87). Despite the strong tidal perturbation, ram pressure is the dominant effect on the observed gas distribution and kinematics (Vollmer et al. 2005b). A double line profile is observed in CO(2–1) observations. As in the Coma spiral galaxy NGC 4848, one CO line is due to galactic rotation, whereas the second CO line is most probably due to gas pushed by ram pressure. Recent deep H α observations of the M 86 region ([Fig. 5-17](#); Kenney et al. 2008) revealed a highly complex and disturbed interstellar/intracluster medium. NGC 4438 is connected to M 86 by several faint H α filaments, which suggests a tidal interaction between the two galaxies, as advocated by Kenney et al. (2008). The timescale and the relative galaxy velocities of the two scenarios (encounter with M 86 or NGC 4435) are about the same. The discovery of an ~ 190 -Myr-old starburst in NGC 4435 by Panuzzo et al. (2007) favors the interaction scenario between NGC 4438 and NGC 4435. Together with NGC 4522 (see below), NGC 4438 is the second galaxy which is undergoing strong ram pressure stripping at a location in the Virgo cluster where this would not be expected from a classical model assuming a spherical, smooth, and static Virgo intracluster medium distribution.

8.2.3 Dwarf Galaxies

Two examples of low-mass irregular galaxies, which have undergone recent ram pressure stripping, were found in the Virgo and Coma cluster. RB 199 is a post-starburst dwarf galaxy with a stellar mass of a few $10^9 M_\odot$ in the Coma cluster. Yoshida et al. (2008) found a complex of narrow blue filaments, bright blue knots, and H α -emitting filaments and clouds, which morphologically resembled a complex of “fireballs,” extending up to 80 kpc from RB 199. This galaxy

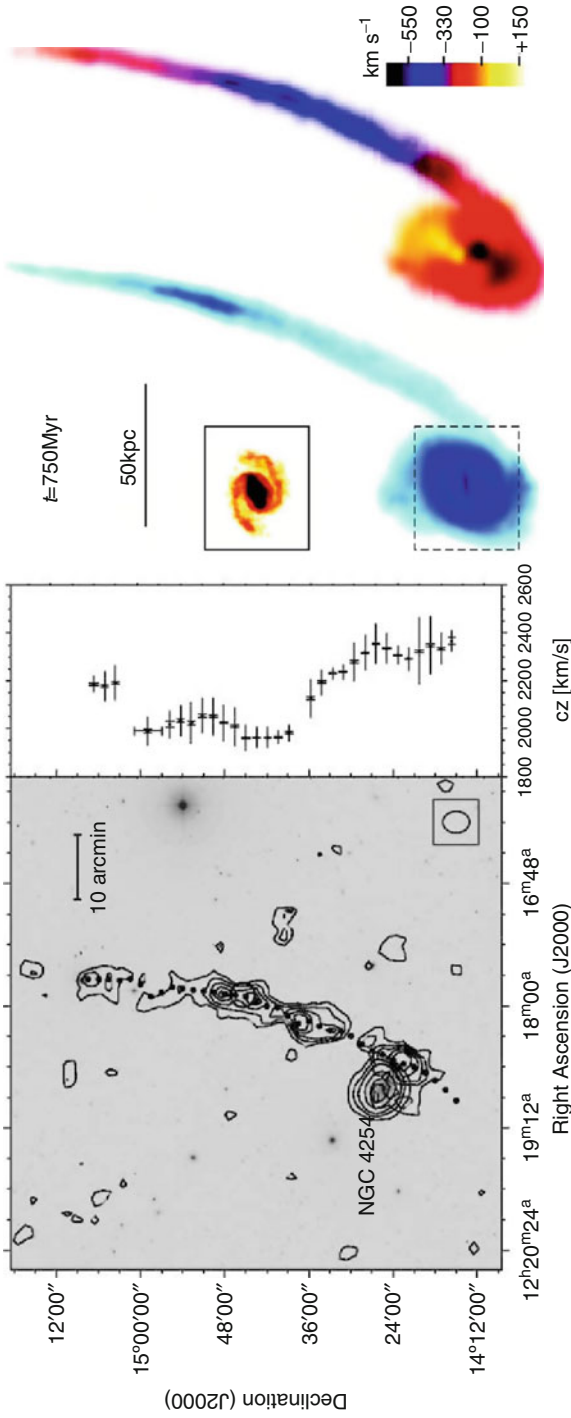
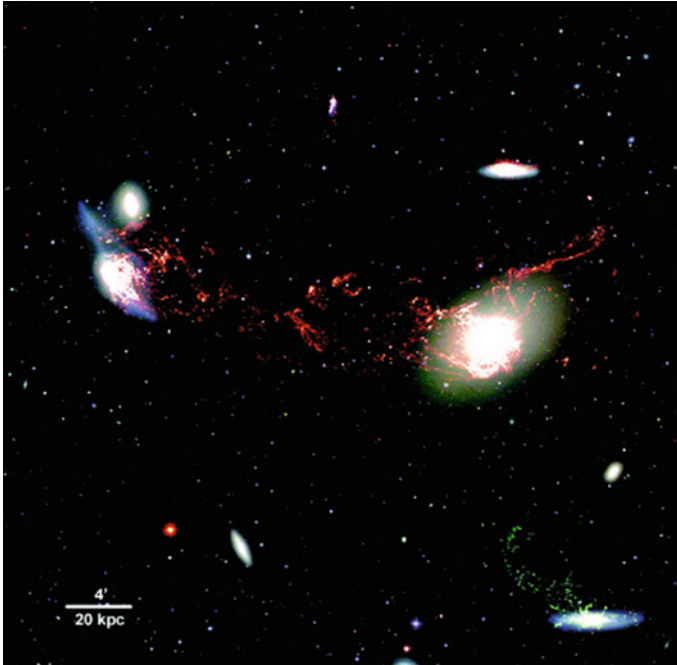


Fig. 5-16

The Virgo cluster spiral NGC 4254. *Left*: Arcicibo HI observations (contour) on an optical image (from Haynes et al. 2008). *Right*: Dynamical model (From Duc and Bournaud 2008)



■ Fig. 5-17

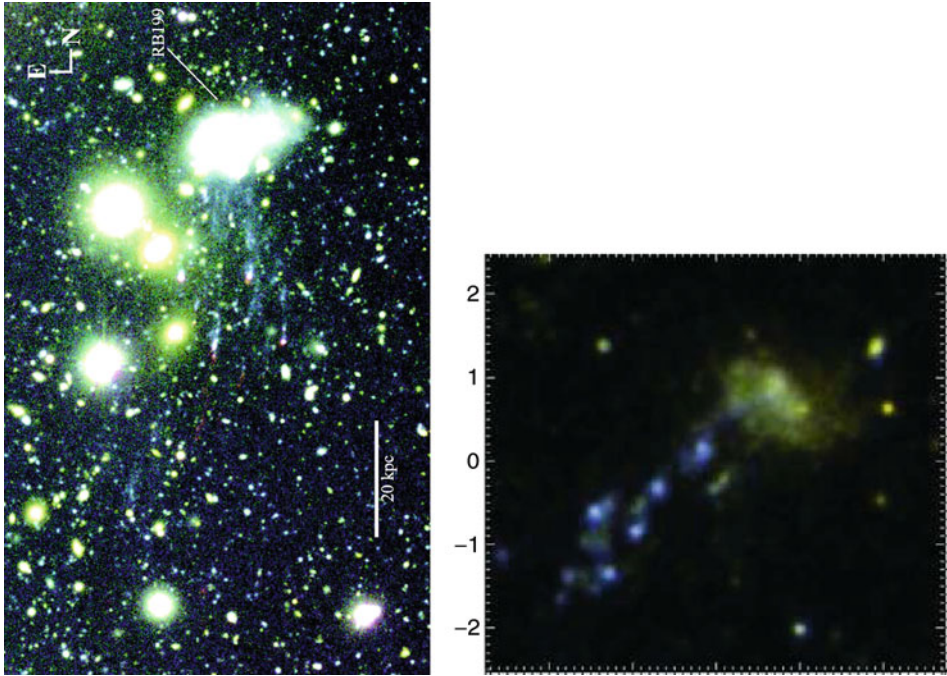
$\text{H}\alpha$ + $[\text{NII}]$ image of M 86 region superposed on a color SDSS gri image. The $\text{H}\alpha$ image is stretched to highlight the faint emission. The “low-velocity” ($< 500 \text{ km s}^{-1}$) $\text{H}\alpha$ + $[\text{NII}]$ emission associated with NGC 4438 is colored *red*, and the “high-velocity” ($> 2,000 \text{ km s}^{-1}$) $\text{H}\alpha$ + $[\text{NII}]$ emission associated with NGC 4388 is colored *green* (From Kenney et al. 2008)

has a highly disturbed morphology indicative of a galaxy–galaxy merger remnant (left panel of Fig. 5-18). The optical colors of the filaments and knots suggest that most of the stars in the fireballs were formed within several times 100 Myr.

The optical morphology of the Virgo cluster dwarf irregular galaxy IC 3428 ($M_* \sim 10^9 M_\odot$) resembles that of RB 199. Hester et al. (2010) found a 17-kpc UV tail of bright knots and diffuse emission behind the galaxy IC 3418 (right panel of Fig. 5-18). $\text{H}\alpha$ imaging confirmed that star formation is ongoing in the tail. The stripped gas thus vigorously formed and still forms stars over the last few 100 Myr. This is in contrast to the low star formation rate in stripped gas tails of late-type galaxies (e.g., Vollmer et al. 2008).

8.3 A Holistic View on Ram Pressure Stripping

A first complete ram pressure stripping time sequence was established by Vollmer (2009; Fig. 5-19). He combined the results of detailed comparisons between dynamical models and observations of the interstellar medium in ram pressure stripped galaxies in the Virgo cluster. According to his analysis, it is possible to observe ram pressure-induced perturbations



■ Fig. 5-18

Ram pressure-stripped galaxies with an optical tail structure. *Left panel:* imaging showing a 17-kpc tail of star formation trailing IC 3418 as it plunges through Virgo's intracluster medium. Color composite ultraviolet image: FUV is *blue*, NUV is *red*, and the average UV intensity is *green*. The y axis scale is in arcmin (from Hester et al. 2010). *Right panel:* false color (B band: *blue*; R_C band: *green*; $H\alpha$: *red*) image of area around RB 199 in the Coma cluster (from Yoshida et al. 2008). A tail structure is visible up to ~ 80 kpc south to RB 199

~ 300 Myr around the galaxy's closest approach to the cluster center, i.e., when peak ram pressure occurs if a spherical, smooth, and static intracluster medium distribution is assumed. The relative brevity of this period compared to the galaxy's orbital timescale (several Gyr) explains the rareness ($\sim 15\%$) of observed ram pressure-induced perturbations in Virgo spiral galaxies.

Observationally, the different stages of ram pressure stripping can be recognized in the following way:

- Increasing, moderately strong ram pressure (>50 Myr before peak, class (i)): moderately truncated HI disk, extraplanar gas of moderate surface density, continuous velocity field between the disk and the extraplanar region, radio-deficient region, and/or ridge of polarized radio continuum emission at the outer gas disk opposite to the extraplanar region, for example, NGC 4501, NGC 4330.
- Ongoing strong ram pressure (near peak, class (ii)): strongly truncated HI disk, extraplanar gas of high surface density, continuous velocity field between the disk and the extraplanar region, radio-deficient region, and/or ridge of

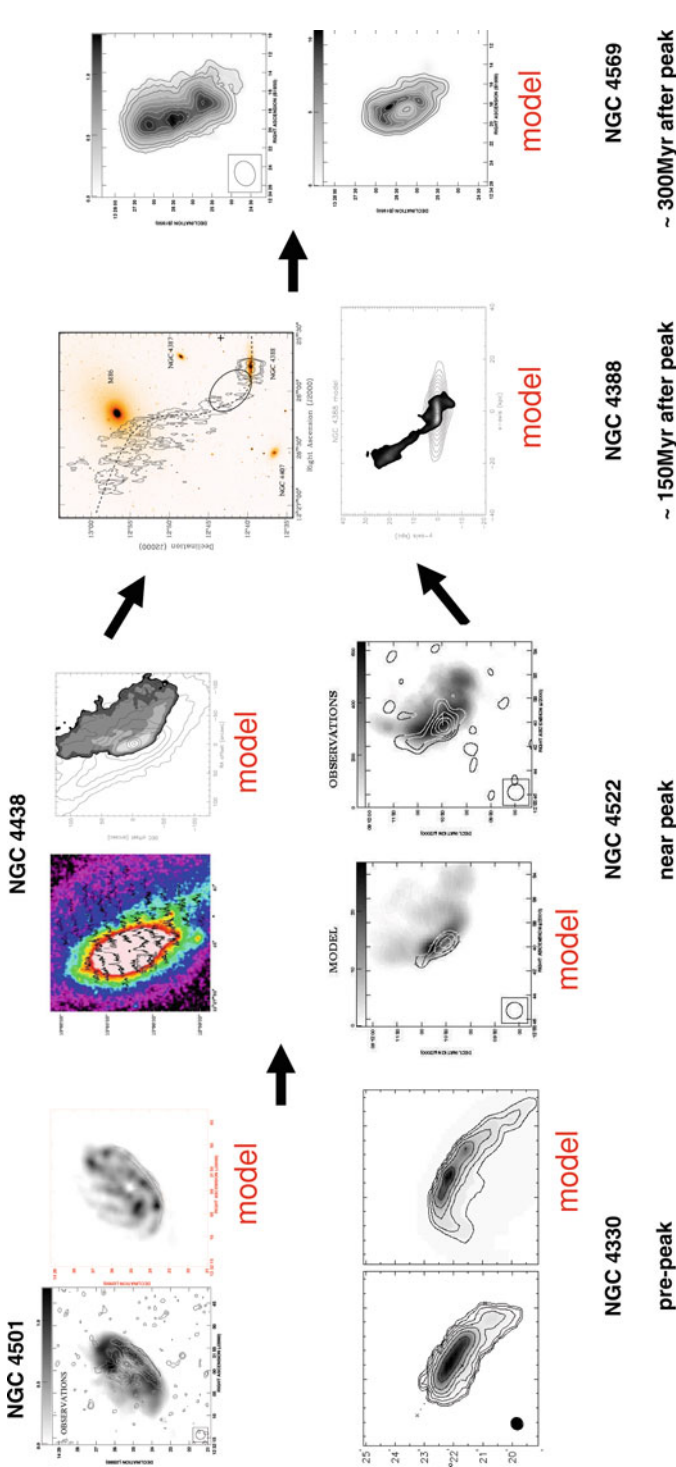


Fig. 5-19

Model-based complete ram pressure stripping time sequence for Virgo cluster spiral galaxies. NGC 4501 (gray scale: H I, contour: polarized radio continuum emission; Vollmer et al. 2008) and NGC 4330 (gray scale and contours: H I; Chung et al. 2007; Vollmer et al. 2012) are approaching the cluster center and are thus in a stage of pre-peak ram pressure (class (i)). NGC 4522 (gray scale: H I, contour: polarized radio continuum emission; Kenney et al. 2004; Vollmer et al. 2006) and NGC 4438 (observations: CO spectra on optical image; model: gray scale: gas surface density; contours: stellar distribution; (Vollmer et al. 2005a) are close to peak ram pressure (class (ii)). NGC 4388 (class (iii); observations: contour: H I Oosterloo and van Gorkom 2005; model: gray scale: gas surface density; contour: stellar distribution; Vollmer and Huchtmeier 2003) and NGC 4569 (class (iv); gray scale and contours: H I; Vollmer et al. 2004a) are leaving the cluster center (From Vollmer 2009)

polarized radio continuum emission at the outer gas disk opposite to the extraplanar region, for example, NGC 4438, NGC 4522.

- Decreasing ram pressure (<200 Myr after peak, class (iii)): strongly truncated HI disk, extended extraplanar gas of low surface density, continuous velocity field between the disk and the extraplanar region, and ridge of polarized radio continuum emission at the outer gas disk opposite to the extraplanar region, for example, NGC 4388.
- Decreasing ram pressure (>200 Myr after peak, class (iv)): strongly truncated HI disk, perturbed outer gas arms, discontinuous velocity field between the disk and the extraplanar region, ridge of polarized radio continuum emission at the outer gas disk opposite to the extraplanar region, and possible ridge of polarized radio continuum emission at the outer gas disk due to shear motions from the resettling gas, for example, NGC 4569.

The dynamical models yield the 3D velocity vector of the galaxies, the peak ram pressures, and the times to peak ram pressure. In the case of a smooth, static, and spherical intracluster medium, peak ram pressure occurs during the galaxy's closest approach to the cluster center, i.e., when the galaxy's velocity vector is perpendicular to its distance vector. Under these conditions, the galaxy's present line-of-sight distance and its 3D position during peak ram pressure can be calculated. The linear orbital segments derived in this way together with the intracluster medium density distribution from Schindler et al. (1999) are consistent within a factor of 2 with the dynamical simulations for NGC 4501, NGC 4330, and NGC 4569. The impact parameters of the galaxy orbits vary between 200 kpc and 600 kpc.

The analysis of multiwavelength photometry and optical spectra of the gas-free outer regions of the galactic disks allow to derive the time since star formation has been quenched by gas removal via ram pressure stripping. Boselli et al. (2006) used multiband photometry and stellar population modeling to constrain the quenching time. Crawl and Kenney (2008) analyzed the stellar populations in these outer disks of 10 Virgo cluster spiral galaxies, using integral field spectroscopy and UV photometry. All of the galaxies with spatially truncated star formation have outer-disk stellar populations consistent with star formation ending within the last 500 Myr. For approximately half of the galaxies, the truncation ages are consistent with galaxies being stripped in or near the cluster core, where simple ram pressure estimates can explain the observed stripping radius. However, the other half of the galaxies were clearly stripped outside the cluster core. Pappalardo et al. (2010) refined the truncation age determination for NGC 4388 using a nonparametric inversion tool to reconstruct the star formation history of a galaxy from deep VLT spectroscopy and multiband photometry. For all three galaxies where star formation truncation ages based on dynamical models exist (NGC 4569, NGC 4388, NGC 4522), they agree with the timescales derived from spectrophotometry.

Finally, the small edge-on galaxy NGC 4522 (► Fig. 5-2) deserves special attention. Its gas disk is strongly truncated and extraplanar high column density gas is present (► Fig. 5-2). Dynamical modeling, the presence of an asymmetric ridge of polarized emission (Vollmer et al. 2004b), and the analysis of the optical spectrum of the gas-free outer disk (Crawl and Kenney 2008) infer strong ongoing ram pressure stripping. However, the galaxy is located at a projected distance of $3.3^\circ \sim 1$ Mpc from the cluster center. Assuming a smooth and static intracluster medium, the calculated ram pressure at this location (► 5.2) appears inadequate by an order of magnitude to cause the observed stripping. The most probable scenario is a dynamic, shock-filled intracluster medium with bulk motions and local density enhancements associated with

the galaxy group around the elliptical galaxy M 49, which falls into the Virgo cluster from the south. Together with NGC 4438 (see [Sect. 8.2.2](#)), NGC 4522 represents a second galaxy which is not classically stripped in the core of the Virgo cluster.

8.3.1 The Response of the Multiphase ISM and Star Formation to Ram Pressure

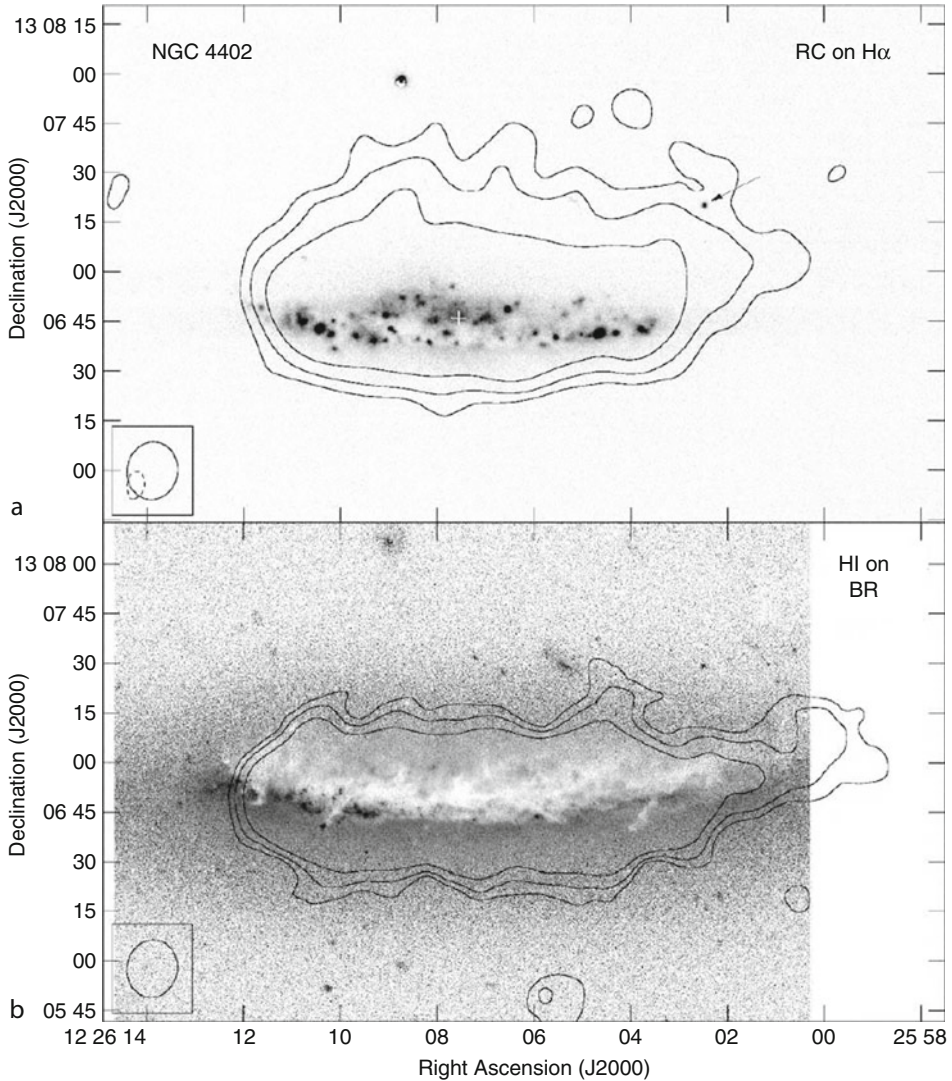
As described in [Sect. 5](#), the interstellar medium consists of different phases. The warm neutral phase is observable in H I line emission and the molecular phase in CO line emission. H α emission traces the dense warm ionized medium (diffuse gas or H II regions) and diffuse X-ray emission the hot ionized gas phase. In addition, synchrotron emission from cosmic ray gas and the magnetic field is detected in the radio continuum.

Tidal interactions act in the same way on all gas phases and on the stellar component. Ram pressure only affects the ISM. The acceleration of gas clumps by ram pressure depends on their surface density,

$$a = \frac{p_{\text{ram}}}{\Sigma_{\text{ISM}}} = \frac{\rho_{\text{ICM}} v_{\text{gal}}^2}{\Sigma_{\text{ISM}}}, \quad (5.11)$$

where p_{ram} is the ram pressure, ρ_{ICM} the intracluster medium density, v_{gal} the galaxy velocity with respect to the intracluster medium, and Σ_{ISM} the ISM surface density. Clouds with higher surface densities are thus less affected by ram pressure than clouds with low surface densities. There is evidence that this is actually the case. The edge-on Virgo spiral galaxy NGC 4402 ([Fig. 5-20](#)) shows signs of ongoing ram pressure stripping ([Crowl et al. 2005](#)): the H I disk is strongly truncated and a short H I tail is observed. Moreover, the radio continuum halo is compressed on one side of the galactic disk. Deep optical images show a remarkable dust lane morphology: at half the optical radius, the dust lane of the galaxy curves up and out of the disk. On the leading eastern edge of the interaction, the H I contours appear to cut off inside the dust distribution, suggesting that the less dense gas in this part of the galaxy has already been stripped. To the south of the galactic disk, where the galaxy is relatively clean of gas and dust, there are 1-kpc-long linear dust filaments with a position angle that matches the shape of the radio continuum halo. One of the observed dust filaments has an H II region at its head. These dust filaments are interpreted as large, dense clouds that were initially left behind as the low-density interstellar medium was stripped but were then ablated by the ram pressure wind. The same phenomenon of massive dense molecular clouds which decouple from the ram pressure wind is observed in NGC 4522 and NGC 4438. Both galaxies undergo strong active ram pressure stripping. In both galaxies, small amounts of molecular gas ($\sim 10^7 M_{\odot}$) with very narrow linewidths are observed in H I-free regions where the bulk of the gas has been removed by ram pressure: in the northern tail of NGC 4438 ([Vollmer et al. 2005b](#)) and in NGC 4522 beyond the gas truncation radius ([Vollmer et al. 2008](#)). There is one indication that the diffuse warm ionized gas is stripped more efficiently than molecular gas: in the region where extraplanar gas is detected in NGC 4438, the radial velocities of the diffuse H α emission are significantly offset from ($\Delta v \geq 40 \text{ km s}^{-1}$), whereas the velocities of the H II regions follow those of the molecular gas ([Vollmer et al. 2009](#)).

The evidence of extraplanar star formation is rare in ram pressure stripped Virgo spiral galaxies. Some extraplanar H II regions are detected in Virgo spiral galaxies with H I tails: NGC 4402 ([Cort ese et al. 2004](#)), NGC 4438 ([Kenney et al. 1995](#)), NGC 4388



■ Fig. 5-20

The Virgo cluster spiral galaxy NGC 4402. *Upper panel:* H α image together with the outer three radio continuum contours. The arrow marks an extraplanar H II region discovered by Cortés et al. (2004). *Lower panel:* B – R image showing the distribution of dust lanes in the galaxy, along with the outer three HI contours. The kpc dust lanes stick out from the southern edge of the galactic disk and run to the southeast (From Crowl et al. 2005)

(Yoshida et al. 2004), NGC 4522 (Kenney et al. 2004), and NGC 4330 (Abramson et al. 2011). Based on their dynamical model, Vollmer et al. (2008) suggested the following ram pressure stripping scenario: a significant part of the gas is stripped in the form of overdense armlike structures. Molecules and stars form within this dense gas according to the same laws as in

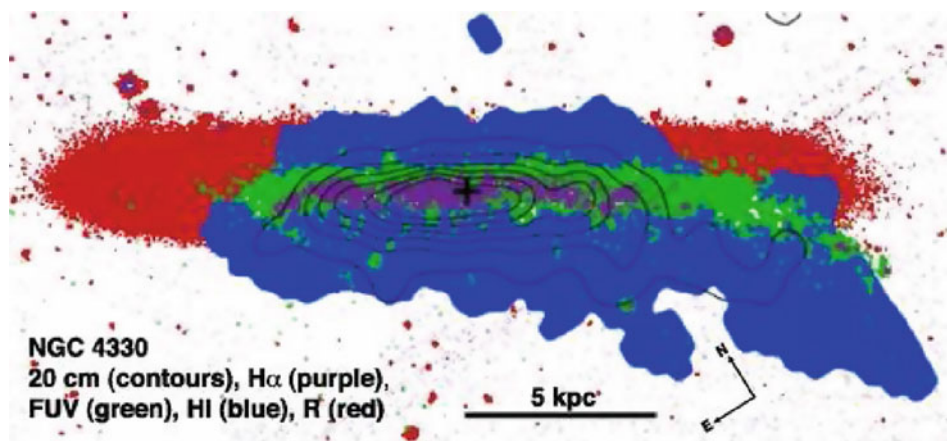


Fig. 5-21

NGC 4330 schematic showing the distributions of R (red), FUV (green), H α (purple), HI (blue), and 20-cm radio continuum (contours). The radio continuum and HI tails are displaced downwind (SE) of the UV and H α tails, indicating that the ISM in this area has been pushed downwind over time (From Abramson et al. 2011)

the galactic disk, i.e., they mainly depend on the total large-scale gas density. Star formation proceeds where the local large-scale gas density is highest. In the absence of a confining gravitational potential, the stripped gas arms will most probably disperse; i.e., the density of the gas will decrease and star formation will cease. This might have happened in NGC 4330 where Abramson et al. (2011) discovered an offset between the UV and HI tails (Fig. 5-21). This offset can be explained with the following scenario: since collapsing and star-forming gas clouds decouple from the ram pressure wind, the UV-emitting young stars have the angular momentum of the gas at the time of their creation. On the other hand, the gas is constantly pushed by ram pressure and its density decreases. At a certain density threshold, star formation ceases in the displaced gas. The observed gas tails has a very low present star formation efficiency. The UV emission indicates that the past star formation efficiency (~ 100 Myr) was much higher.

9 The Detailed Picture

It is difficult to find cluster spiral galaxies with clear signs of ongoing ram pressure stripping and unambiguous examples are rare. The signposts of ram pressure stripping are (i) a symmetric old stellar disk together with a gas disk truncated inside the optical radius, (ii) a one-sided gas tail, and (iii) a radio-deficient region and/or an asymmetric polarized radio continuum ridge located in the outer gas disk opposite to the gas tail. In the absence of a long gas tail, it is easier to recognize extraplanar gas in edge-on galaxies. Therefore, we are somewhat biased against this particular projection. Although the distortions of the gas distribution can be quite dramatic, the gas velocity field is still smooth and regular. In the Virgo cluster, these asymmetries can be observed during ~ 300 Myr, compared to an orbital timescale of a few Gyr. This partly explains the rareness of published cases with ongoing ram pressure stripping. In the classical picture,

a galaxy approaches the cluster center on a highly eccentric orbit. The intracluster medium is in hydrostatic equilibrium and does not move. Ram pressure stripping thus occurs close to the cluster core when (► 5.2) is fulfilled. The distance from the cluster center where a significant amount of gas is removed from the galaxy depends on the radial distribution of intracluster medium which can be very different from cluster to cluster (e.g., Virgo and Coma). We have learned from the Virgo spiral galaxy NGC 4522 that ram pressure stripping can occur far away from the cluster center in regions where classical ram pressure by a static intracluster medium is insufficient. The explanation is that the intracluster medium is moving at a high speed in the opposite direction of the galaxy's motion. Since ram pressure depends on the square of the intracluster medium velocity with respect to galaxy, this can dramatically enhance ram pressure. Thus, whenever the intergalactic medium of a subcluster or galaxy group collides with the intracluster medium of the main cluster during a cluster–subcluster or a cluster–group merger, ram pressure stripping can occur at the cluster periphery provided that there are galaxies which move against the direction of the infalling intergalactic medium.

The detailed comparison between dynamical models and gas distributions and velocity fields of Virgo spiral galaxies showed that the Gunn and Gott criterion (► 5.2) is valid within a factor of 2 (Vollmer 2009). The models of different types (3D hydro, SPH, sticky particles) agree in this respect (see ► Sect. 4). It is not enough to reproduce the observed gas distribution, because the results can be ambiguous. The observed gas velocity field adds important constraints for the modeling. The motions in the plane of the sky can be probed via the polarized radio continuum emission which is sensitive to compression and shear. The main ingredients of ram pressure stripping are (i) ram pressure; (ii) galactic rotation; (iii) gas shadowing, i.e., gas on the windward side can shadow gas located on the downwind side; and (iv) for long gas tails intracluster medium – ISM mixing. Mixing requires Kelvin–Helmholtz instabilities and can thus only be simulated by 3D Eulerian hydrodynamics.

Most of the gas tails are observed in H α and only a few in X-rays, H α , and radio continuum emission. Unfortunately, there is only one simultaneous detection of a gas tail in H α and X-rays, NGC 4848 in the Coma cluster. Why do some tails are X-ray bright and form more stars (ESO 137-001 in Abell 3627) than others (NGC 4388 in Virgo) which are fainter in X-rays? Tonnesen et al. (2011) suggested that the primary requirement is a high-pressure intracluster medium. This is because the stripped tail is mostly in pressure equilibrium with the intracluster medium, but mixing leaves it with densities and temperatures intermediate between the cold gas in the disk and the hot intracluster medium. Given a high enough intracluster medium pressure, the mixed gas lies in the X-ray bright region of the phase diagram. This suggestion is consistent with the higher intracluster medium temperature and thus pressure of Abell 3627. This also explains why the X-ray bright tail of ESO 137-001 shows diffuse H α emission.

The work on NGC 4522 and NGC 4330 suggests that the gas is stripped in an arm structure with high densities. As long as the gas is of high density, it forms stars. Once the gas is pushed out of the galactic disk, the gravitational confinement vanishes and the bulk of the gas expands and is mixed into the tenuous hot intracluster medium. Since the stripping timescale is long compared to the lifetime of a molecular cloud, the ISM is stripped as an entity. Only the largest molecular cloud complexes might decouple from the ram pressure wind and stay behind (NGC 4522, ► Fig. 5-2; NGC 4402, ► Fig. 5-20, NGC 4438 in the Virgo cluster). There are indications for a modest enhancement of the star formation rate per surface area in NGC 4522 (Crowl and Kenney 2006). At the same time, the total star formation rate of the galaxy is reduced because of the truncation of the gas and star-forming disk. Thus, whereas the local star formation rate can be enhanced up to a factor of a few during a ram pressure stripping event, the total star formation rate decreases in most cases.

The gas stripping of gas-rich dwarf irregular galaxies proceeds in a different way. The star formation efficiency of the stripped gas is higher leading to stellar tails which are observable in the UV and optical domain (RB 199 in Coma and IC 3418 in Virgo).

Gravitational interactions, like close flybys of massive galaxies, can loosen the gas from the galaxy's gravitational potential, making ram pressure stripping more efficient (NGC 4654, [Fig. 5-15](#); NGC 4438 in the Virgo cluster). In an extreme case, a gravitational interaction might even be responsible for a 100-kpc gas tail (NGC 4254 in the Virgo cluster; [Fig. 5-16](#)).

The end-product of ram pressure stripping are spiral galaxies with a truncated gas and star-forming disk. These stripped late-type galaxies can easily be misclassified as early-type spirals (Koopmann and Kenney 1998). Star formation will then consume the gas, the gas surface density and star formation rate will decrease, and the galaxy will become passive or anemic (NGC 4548, NGC 4579, NGC 4569 in the Virgo cluster). After the stripping, the outer gas-free disk has a post-starburst spectrum with strong Balmer absorption lines and no significant emission from ongoing star formation (Crowl and Kenney 2006).

For the transformation of the spiral galaxies into lenticulars, a morphological transformation leading to larger bulges seems to be necessary as discussed in [Sect. 7](#). Tidal interactions are the prime candidate for this transformation which happened either via slow encounters in a group environment before infall into the galaxy cluster or via harassment or single close flybys of massive galaxies in the cluster environment. An example for an ongoing spiral-S0 transformation at the cluster periphery is the Virgo cluster galaxy NGC 4438. A single gravitational interaction leads to important stellar tidal tails ([Fig. 5-17](#)). Once the galaxy has passed the cluster core, these tails will be stripped by the gravitational potential of the cluster and NGC 4438 will resemble an S0 galaxy. The tidally stripped stars will contribute to the diffuse intracluster light (see, e.g., Mihos et al. 2005).

10 A Local View on the Butcher–Oemler Effect

Butcher and Oemler (1984) were the first to report an increasing fraction of blue galaxies in 33 rich galaxy clusters out to a redshift of $z \sim 0.5$. Subsequent studies showed similar trends for the star formation rate (e.g., Balogh et al. 1999; Poggianti et al. 2006) and galaxy morphology (e.g., Dressler et al. 1997; Treu et al. 2003), or spectral properties (Ellingson et al. 2001). The fraction of blue spirals is determined by the cluster richness and redshift (Margoniner et al. 2001). This global effect can be understood in a scenario where the rate of field galaxy infall onto clusters decreases with decreasing redshift (Kauffmann 1995; Abraham et al. 1996; Ellingson et al. 2001). Since the mean cluster mass increases with decreasing redshift, the specific infall rate per unit cluster mass decreases at an even faster rate. Furthermore, because of the sharply declining global star formation rate as a function of decreasing redshift (Hopkins and Beacom 2006), field galaxies form on average more stars and are bluer at higher redshifts. A more detailed view of the Butcher–Oemler effect is that of a significant evolution in the fractional population gradient of early- and late-type galaxies (Ellingson et al. 2001). Both low- and high-redshift clusters have similar populations in the cluster cores, but higher redshift clusters have steeper gradients and more star-forming galaxies at radii outside of the core region. The blue galaxy fraction at a given redshift depends on cluster mass (richness, Margoniner et al. 2001; X-ray temperature Urquhart et al. 2010), but its gradient with respect to redshift is approximately the same for all clusters (Margoniner et al. 2001). The Butcher–Oemler effect thus has an environmental

and a cosmological component. The main effect of the cluster environment is to quench star formation of the infalling galaxies, and more massive galaxy clusters are more efficient in stopping the star formation of their galaxies. The cause of the environmental component of the Butcher–Oemler effect (ram pressure stripping or tidal interactions) has still to be determined. It is well possible that both effects are equally needed. The local view of the cosmological component of the Butcher–Oemler effect is that the fraction of dynamically young clusters as the Virgo, Abell 1367, and Norma clusters with a high infall rate of blue field galaxies increases with redshift.

The studies of local galaxy clusters teach us that cluster environments can be very different. In a tentative sequence for cluster evolution, a galaxy cluster begins as a Fornax-like cluster with a high fraction of healthy spirals and a small amount of hot intracluster medium peaking on the central luminous galaxy. In this environment, gravitational interactions dominate and ram pressure stripping does not play a role for galaxy evolution within the cluster. When important groups of galaxies fall into the cluster, it will look like the Virgo cluster with a spiral-rich galaxy distribution which shows a lot of substructure. If the infalling groups contain a significant amount of hot intragroup gas, the intracluster–intragroup gas merging will heat the intracluster medium and lead to important bulk motions. In these highly dynamic environment with increasing intracluster medium mass, ram pressure becomes more and more efficient. Ram pressure typically begins to affect the galaxies' outer gas disks inside the cluster's Virial radius. The clustercentric distance from which ram pressure significantly reduces the galaxies' gas and star-forming disks depends on (i) the central density and core radius of the intracluster medium distribution and (ii) the intracluster medium bulk motions. Only galaxies on eccentric orbits, leading them deeply into the cluster core or galaxies flying against bulk motions will be stripped efficiently. The gas stripping is then quasi-instantaneous. For the other galaxies on less eccentric orbits close flybys of massive perturbers can loosen the gas in the outer parts of the disk which can then be stripped by a relatively small amount of ram pressure. The timescale for this mixed interaction is longer and depends on the probability of a close gravitational interaction. Galaxy harassment, or multiple close flybys, mainly changes the morphology of low-mass galaxies. In addition, spiral galaxies consume their gas via star formation without a supply of fresh gas. The galaxy cluster grows steadily in this way.

If another smaller galaxy cluster with a significant amount of intracluster gas hits the main cluster, the intracluster medium temperature and bulk motions increase. With increasing mass and temperature of the intracluster medium, its central density and core radius increase (Jones and Forman 1999; Schindler et al. 1999). We then have a cluster-like the Norma or Abell 1367 clusters where ram pressure stripping is enhanced in the gas merger region. When the intracluster medium is relaxed again, the cluster will look like the Coma cluster. Through the dynamical buildup of the intracluster medium, ram pressure becomes more and more important for the evolution of the star formation of cluster galaxies. Ram pressure stripped spirals consume the residual gas and the spiral galaxy becomes passive or anemic. The end products might be relatively faint lenticular galaxies.

Global morphological transformation of spiral galaxies into lenticulars within the cluster environment certainly needs important tidal interactions. It should not be forgotten that some galaxies are already preprocessed within infalling groups, where they have already lost a fraction of their ISM and might have changed morphology. The formation of lenticular galaxies is thus a heterogeneous process which acts in group and cluster environments (see also Moran et al. 2007; van den Bergh 2009).

11 Conclusions and Outlook

We have seen that the environment modifies the properties of a galaxy. The primary effects are gas removal, quenching of star formation, and a possible morphological transformation. Those galaxies that live in a group undergo predominantly slow tidal interactions with other galaxies. Because of their high galaxy density, compact groups show dramatic tidal tails and galaxy mergers. In rare cases, ram pressure can play a role, if a galaxy flies through a gaseous tidal tail or if the group contains a considerable amount of intragroup gas. The end product of a galaxy merger is a lenticular or elliptical galaxy. Tidal interactions will drive the ISM of the inner disk into the galaxy center and loosen the ISM of the outer disk. Star formation then consumes the ISM in the galactic disk. In this way, some group galaxies can become HI deficient and/or undergo morphological transformation.

A significant fraction of galaxies are preprocessed in a group environment before falling into a cluster. In galaxy clusters, tidal interactions are fast and numerous (galaxy harassment). These interactions will mainly modify the morphology of low-mass galaxies. If the intracluster gas mass is high and the core radius of its distribution is large, or if the intracluster medium is moving due to a cluster–cluster merger, ram pressure stripping becomes an important agent of galaxy evolution. Ram pressure stripping is most efficient for galaxies on highly eccentric orbits and for galaxies moving against bulk motions of the intracluster gas. The galaxies' ISM is then removed instantaneously according to the Gunn and Gott criterion (☉ 5.2), and the galaxies become HI deficient. There is now evidence in local galaxy clusters where and how ram pressure acts on a spiral galaxy. Tidal interactions and ram pressure stripping can act simultaneously, enhancing the ISM removal. These mixed interactions occur preferentially at the cluster periphery (≥ 1 Mpc). Signs of ram pressure stripping can be detected up to about one virial radius of the cluster. The time window, in which we can unambiguously identify the effects of ram pressure stripping, is small compared to the orbital period. Therefore, it is not easy to find these galaxies in a cluster. Large imaging HI surveys are particularly useful to identify ram pressure stripping candidates. Polarized radio continuum observations can be used to verify the ram pressure stripping hypothesis. The physics of the interaction can then be studied by multiwavelength observations from the X-ray to radio domain. For a limited sample of galaxies, it is now possible to constrain their 3D orbits and interaction histories within the cluster. We are now at the point where we can study the reaction (phase change, star formation) of the multiphase ISM (molecular, atomic, ionized) to ram pressure.

For the moment, detailed interaction diagnostics are limited to local galaxy clusters where the resolution of current telescopes is sufficiently high. The HI imaging resolution for Coma galaxies is already too coarse to permit detailed modeling. Furthermore, the most distant galaxy clusters where galaxies could be detected (not resolved) in HI emission are at $z = 0.2$ (Abell 963, Abell 2192; Verheijen et al. 2007). The main obstacles to observing HI in distant galaxies are the necessarily long integration times and man-made interference outside the protected 21-cm band. The square kilometer array (SKA) will entirely change this situation, allowing us detailed HI line and radio continuum imaging of cluster galaxies in local clusters beyond Virgo and giving us access to the gas content of galaxies at higher redshifts. With ALMA, it will be possible to study the reaction of the dense gas phase to ram pressure stripping (the decoupling of giant molecular clouds from the ram pressure wind) and investigate the total molecular gas content of spiral galaxies in clusters beyond the local universe. LOFAR will give us access to the population of older cosmic ray electrons. This will greatly increase our knowledge on the

effects of ram pressure stripping on the cosmic ray gas. The Herschel satellite has already and will improve our understanding of the role of dust in environmental interactions. The road to a better understanding of environmental effects on galaxy evolution is thus lined with beautiful upcoming instruments.

Acknowledgments

I would like to thank A. Boselli and J. Köppen for their careful reading of the manuscript and useful remarks and discussions.

References

- Abadi, M. G., Moore, B., & Bower, R. G. 1999, *MNRAS*, 308, 947
- Abraham, R. G. et al. 1996, *ApJ*, 471, 694
- Abramson, A., Kenney, J. D. P., Crowl, H. H., Chung, A., van Gorkom, J. H., Vollmer, B., & Schiminovich, D. 2011, *AJ*, 141, 164
- Allam, S., Assendorp, R., Longo, G., Braun, M., & Richter, G. 1996, *A&AS*, 117, 39
- Andersen, V., & Owen, F. N. 1995, *AJ*, 109, 1582
- Balogh, M. L., Morris, S. L., Yee, H. K. C., Carlberg, R. G., & Ellingson, E. 1999, *ApJ*, 527, 54
- Balogh, M. L., Baldry, I. K., Nichol, R., Miller, C., Bower, R., & Glazebrook, K. 2004, *ApJ*, 615, L101
- Balsara, D., Livio, M., & O'Dea, C. P. 1994, *ApJ*, 437, 83
- Bamford, S. P., Rojas, A. L., Nichol, R. C., Miller, C. J., Wasserman, L., Genovese, C. R., & Freeman, P. E. 2008, *MNRAS*, 391, 607
- Barnes, J. E., & Hernquist, L. 1996, *ApJ*, 471, 115
- Barway, S., Wadadekar, Y., Kembhavi, A. K., & Mayya, Y. D. 2009, *MNRAS*, 394, 1991
- Beck, R. 2001, *SSRv*, 99, 243
- Beck, R. 2005, *LNP*, 664, 41
- Bekki, K., Couch, W. J., & Drinkwater, M. J. 2001, *ApJ*, 552, L105
- Bekki, K., Couch, W. J., & Shioya, Y. 2002, *ApJ*, 577, 651
- Bicay, M. D., & Giovanelli, R. 1987, *ApJ*, 321, 645
- Bigiel, F., Leroy, A., Walter, F., Brinks, E., de Blok, W. J. G., Madore, B., & Thornley, M. D. 2008, *AJ*, 136, 2846
- Billier, B. A., Jones, C., Forman, W. R., Kraft, R., & Ensslin, T. 2004, *ApJ*, 613, 238
- Binggeli, B., Sandage, A., & Tammann, G. A. 1988, *ARA&A*, 26, 509
- Binggeli, B., Tarenghi, M., & Sandage, A. 1990, *A&A*, 228, 42
- Biviano, A. 1998, Untangling Coma Berenices: a new vision of an old cluster, in Proceedings of the Meeting held in Marseilles (France), June 17–20, 1997, ed. A. Mazure, F. Casoli, F. Durret, & D. Gerbal (Word Scientific Publishing Co Pte Ltd, Singapore), 1
- Blanton, M. R., & Moustakas, J. 2009, *ARA&A*, 47, 159
- Böhringer, H., Briel, U. G., Schwarz, R. A., Voges, W., Hartner, G., & Trümper, J. 1994, *Nature*, 368, 828
- Böhringer, H., Neumann, D. M., Schindler, S., & Kraan-Korteweg, R. C. 1996, *ApJ*, 467, 168
- Boselli, A., & Gavazzi, G. 2006, *PASP*, 118, 517
- Boselli, A., Gavazzi, G., Lequeux, J., Buat, V., Casoli, F., Dickey, J., & Donas, J. 1995, *A&A*, 300, L13
- Boselli, A., Mendes de Oliveira, C., Balkowski, C., Cayatte, V., & Casoli, F. 1996, *A&A*, 314, 738
- Boselli, A., Lequeux, J., & Gavazzi, G. 2002, *A&A*, 384, 33
- Boselli, A., Boissier, S., Cortese, L., Gil de Paz, A., Seibert, M., Madore, B. F., Buat, V., & Martin, D. C. 2006, *ApJ*, 651, 811
- Boselli, A., Boissier, S., Cortese, L., & Gavazzi, G. 2008, *ApJ*, 674, 74
- Boulares, A., & Cox, D. P. 1990, *ApJ*, 365, 544
- Bravo-Alfaro, H., Cayatte, V., van Gorkom, J. H., & Balkowski, C. 2000, *AJ*, 119, 580
- Briel, U. G., Henry, J. P., & Böhringer, H. 1992, *A&A*, 259, L31
- Broeils, A. H., & Rhee, M.-H. 1997, *A&A*, 324, 877
- Butcher, H., & Oemler, A., Jr. 1978, *ApJ*, 226, 559
- Butcher, H., & Oemler, A., Jr. 1984, *ApJ*, 285, 426
- Byrd, G., & Valtonen, M. 1990, *ApJ*, 350, 89
- Casoli, F., Boisse, P., Combes, F., & Dupraz, C. 1991, *A&A*, 249, 359
- Casoli, F., Dickey, J., Kazes, I., Boselli, A., Gavazzi, P., & Baumgardt, K. 1996, *A&A*, 309, 43

- Cayatte, V., van Gorkom, J. H., Balkowski, C., & Kotanyi, C. 1990, *AJ*, 100, 604
- Cayatte, V., Kotanyi, C., Balkowski, C., & van Gorkom, J. H. 1994, *AJ*, 107, 1003
- Chamaraux, P., Balkowski, C., & Gerard, E. 1980, *A&A*, 83, 38
- Chilingarian, I., Cayatte, V., Revaz, Y., Dodonov, S., Durand, D., Durret, F., Micol, A., & Slezak, E. 2009, *Sci*, 326, 1379
- Chilingarian, I. V., Mieske, S., Hilker, M., & Infante, L. 2011, *MNRAS*, 412, 1627
- Christlein, D., & Zabludoff, A. I. 2004, *ApJ*, 616, 192
- Chung, A., van Gorkom, J. H., Kenney, J. D. P., & Vollmer, B. 2007, *ApJ*, 659, L115
- Chung, A., van Gorkom, J. H., Kenney, J. D. P., Crowl, H., & Vollmer, B. 2009, *AJ*, 138, 1741
- Clemens, M. S., Alexander, P., & Green, D. A. 2000, *MNRAS*, 312, 236
- Combes, F., Dupraz, C., Casoli, F., & Pagani, L. 1988, *A&A*, 203, L9
- Cortés, J. R., Kenney, J. D. P., & Hardy, E. 2006, *AJ*, 131, 747
- Cortése, L., Gavazzi, G., Boselli, A., & Iglesias-Paramo, J. 2004, *A&A*, 416, 119
- Cortése, L., Gavazzi, G., Boselli, A., Franzetti, P., Kennicutt, R. C., O'Neil, K., & Sakai, S. 2006, *A&A*, 453, 847
- Cortése, L., et al. 2010a, *A&A*, 518, L63
- Cortése, L., et al. 2010b, *A&A*, 518, L49
- Côté, P., et al. 2006, *ApJS*, 165, 57
- Croston, J. H., Hardcastle, M. J., & Birkinshaw, M. 2005, *MNRAS*, 357, 279
- Crowl, H. H., & Kenney, J. D. P. 2006, *ApJ*, 649, L75
- Crowl, H. H., & Kenney, J. D. P. 2008, *AJ*, 136, 1623
- Crowl, H. H., Kenney, J. D. P., van Gorkom, J. H., & Vollmer, B. 2005, *AJ*, 130, 65
- Dame, T. M., Hartmann, D., & Thaddeus, P. 2001, *ApJ*, 547, 792
- Davies, R. D., & Lewis, B. M. 1973, *MNRAS*, 165, 231
- Davies, J. I., et al. 2010, *A&A*, 518, L48
- da Rocha, C., & Mendes de Oliveira, C. 2005, *MNRAS*, 364, 1069
- de la Rosa, I. G., de Carvalho, R. R., Vazdekis, A., & Barbu, B. 2007, *AJ*, 133, 330
- Dickey, J. M., & Gavazzi, G. 1991, *ApJ*, 373, 347
- Domainko, W., et al. 2006, *A&A*, 452, 795
- Donnelly, R. H., Markevitch, M., Forman, W., Jones, C., David, L. P., Churazov, E., & Gilfanov, M. 1998, *ApJ*, 500, 138
- Dressler, A. 1980, *ApJ*, 236, 351
- Dressler, A. 1986, *ApJ*, 301, 35
- Dressler, A. 2004, in *Clusters of Galaxies: Probes of Cosmological Structure and Galaxy Evolution, from the Carnegie Observatories Centennial Symposia*, Carnegie Observatories Astrophysics Series, ed. J. S. Mulchaey, A. Dressler, & A. Oemler (Cambridge, UK: Cambridge University Press), 206
- Dressler, A., & Sandage, A. 1983, *ApJ*, 265, 664
- Dressler, A., et al. 1997, *ApJ*, 490, 577
- Dressler, A., Smail, I., Poggianti, B. M., Butcher, H., Couch, W. J., Ellis, R. S., & Oemler, A., Jr. 1999, *ApJS*, 122, 51
- Drinkwater, M. J., Jones, J. B., Gregg, M. D., & Phillipps, S. 2000, *PASA*, 17, 227
- Drinkwater, M. J., Gregg, M. D., & Colless, M. 2001, *ApJ*, 548, L139
- Duc, P.-A., & Bournaud, F. 2008, *ApJ*, 673, 787
- Duc, P.-A., Bournaud, F., & Masset, F. 2004, *A&A*, 427, 803
- Dunn, L. P., & Jerjen, H. 2006, *AJ*, 132, 1384
- Eke, V. R., Baugh, C. M., Cole, S., Frenk, C. S., King, H. M., & Peacock, J. A. 2005, *MNRAS*, 362, 1233
- Ellingson, E., Lin, H., Yee, H. K. C., & Carlberg, R. G. 2001, *ApJ*, 547, 609
- Fasano, G., Poggianti, B. M., Couch, W. J., Bettoni, D., Kjærgaard, P., & Moles, M. 2000, *ApJ*, 542, 673
- Ferguson, H. C., & Binggeli, B. 1994, *A&ARv*, 6, 67
- Finoguenov, A., Pietsch, W., Aschenbach, B., & Miniati, F. 2004a, *A&A*, 415, 415
- Finoguenov, A., Briel, U. G., Henry, J. P., Gavazzi, G., Iglesias-Paramo, J., & Boselli, A. 2004b, *A&A*, 419, 47
- Forman, W., Schwarz, J., Jones, C., Liller, W., & Fabian, A. C. 1979, *ApJ*, 234, L27
- Fryxell, B., et al. 2000, *ApJS*, 131, 273
- Fumagalli, M., & Gavazzi, G. 2008, *A&A*, 490, 571
- Gaetz, T. J., Salpeter, E. E., & Shaviv, G. 1987, *ApJ*, 316, 530
- Gavazzi, G. 1987, *ApJ*, 320, 96
- Gavazzi, G. 1989, *ApJ*, 346, 59
- Gavazzi, G., & Boselli, A. 1999a, *A&A*, 343, 86
- Gavazzi, G., & Boselli, A. 1999b, *A&A*, 343, 93
- Gavazzi, G., Contursi, A., Carrasco, L., Boselli, A., Kennicutt, R., Scodreggio, M., & Jaffe, W. 1995, *A&A*, 304, 325
- Gavazzi, G., Marcelin, M., Boselli, A., Amram, P., Vilchez, J. M., Iglesias-Paramo, J., & Tarengi, M. 2001, *A&A*, 377, 745
- Gavazzi, G., Boselli, A., van Driel, W., & O'Neil, K. 2005, *A&A*, 429, 439
- Gavazzi, G., Boselli, A., Cortese, L., Arosio, I., Gallazzi, A., Pedotti, P., & Carrasco, L. 2006a, *A&A*, 446, 839
- Gavazzi, G., O'Neil, K., Boselli, A., & van Driel, W. 2006b, *A&A*, 449, 929
- Gavazzi, G., et al. 2008, *A&A*, 482, 43
- Geha, M., Guhathakurta, P., & van der Marel, R. P. 2003, *AJ*, 126, 1794

- Gerber, R. A., & Lamb, S. A. 1994, *ApJ*, 431, 604
- Ghigna, S., Moore, B., Governato, F., Lake, G., Quinn, T., & Stadel, J. 1998, *MNRAS*, 300, 146
- Giovanelli, R., & Haynes, M. P. 1985, *ApJ*, 292, 404
- Gómez, P. L., et al. 2003, *ApJ*, 584, 210
- Graham, A. W. 2002, *ApJ*, 568, L13
- Grebenev, S. A., Forman, W., Jones, C., & Murray, S. 1995, *ApJ*, 445, 607
- Gunn, J. E., & Gott, J. R., III 1972, *ApJ*, 176, 1
- Hashimoto, Y., Oemler, A., Jr., Lin, H., & Tucker, D. L. 1998, *ApJ*, 499, 589
- Haynes, M. P., & Giovanelli, R. 1984, *AJ*, 89, 758
- Haynes, M., Arber, T. D., & Verwichte, E. 2008, *A&A*, 479, 235
- Haşegan, M., et al. 2005, *ApJ*, 627, 203
- Helou, G., Soifer, B. T., & Rowan-Robinson, M. 1985, *ApJ*, 298, L7
- Henriksen, M., & Byrd, G. 1996, *ApJ*, 459, 82
- Hester, J. A., et al. 2010, *ApJ*, 716, L14
- Hickson, P., Mendes de Oliveira, C., Huchra, J. P., & Palumbo, G. G. 1992, *ApJ*, 399, 353
- Hilker, M., Infante, L., Vieira, G., Kissler-Patig, M., & Richtler, T. 1999, *A&AS*, 134, 75
- Hilker, M., Baumgardt, H., Infante, L., Drinkwater, M., Evstigneeva, E., & Gregg, M. 2007, *A&A*, 463, 119
- Hinz, J. L., Rieke, G. H., & Caldwell, N. 2003, *AJ*, 126, 2622
- Hopkins, A. M., & Beacom, J. F. 2006, *ApJ*, 651, 142
- Horellou, C., Casoli, F., & Dupraz, C. 1995, *A&A*, 303, 36
- Huchtmeier, W. K. 1997, *A&A*, 325, 473
- Iglesias-Páramo, J., & Vilchez, J. M. 1999, *ApJ*, 518, 94
- Jáchym, P., Palouš, J., Köppen, J., & Combes, F. 2007, *A&A*, 472, 5
- Jáchym, P., Köppen, J., Palouš, J., & Combes, F. 2009, *A&A*, 500, 693
- Jaffe, W., & Gavazzi, G. 1986, *AJ*, 91, 204
- Jeltema, T. E., Mulchaey, J. S., Lubin, L. M., & Fassnacht, C. D. 2007, *ApJ*, 658, 865
- Johnson, K. E., Hibbard, J. E., Gallagher, S. C., Charlton, J. C., Hornschemeier, A. E., Jarrett, T. H., & Reines, A. E. 2007, *AJ*, 134, 1522
- Jones, C., & Forman, W. 1999, *ApJ*, 511, 65
- Kantharia, N. G., Rao, A. P., & Sirothia, S. K. 2008, *MNRAS*, 383, 173
- Kapferer, W., et al. 2007, *A&A*, 466, 813
- Kapferer, W., Kronberger, T., Ferrari, C., Riser, T., & Schindler, S. 2008, *MNRAS*, 389, 1405
- Kauffmann, G. 1995, *MNRAS*, 274, 153
- Kauffmann, G., White, S. D. M., Heckman, T. M., Ménard, B., Brinchmann, J., Charlot, S., Tremonti, C., & Brinkmann, J. 2004, *MNRAS*, 353, 713
- Kenney, J. D., & Young, J. S. 1986, *ApJ*, 301, L13
- Kenney, J. D. P., Rubin, V. C., Planesas, P., & Young, J. S. 1995, *ApJ*, 438, 135
- Kenney, J. D. P., Koopmann, R. A., Rubin, V. C., & Young, J. S. 1996, *AJ*, 111, 152
- Kenney, J. D. P., van Gorkom, J. H., & Vollmer, B. 2004, *AJ*, 127, 3361
- Kenney, J. D. P., Tal, T., Crowl, H. H., Feldmeier, J., & Jacoby, G. H. 2008, *ApJ*, 687, L69
- Kennicutt, R. C., Jr. 1983, *AJ*, 88, 483
- Kennicutt, R. C., Jr. 1998a, *ARA&A*, 36, 189
- Kennicutt, R. C., Jr. 1998b, *ApJ*, 498, 541
- Kern, K. M., Kilborn, V. A., Forbes, D. A., & Koribalski, B. 2008, *MNRAS*, 384, 305
- Kilborn, V. A., Forbes, D. A., Barnes, D. G., Koribalski, B. S., Brough, S., & Kern, K. 2009, *MNRAS*, 400, 1962
- Koopmann, R. A., & Kenney, J. D. P. 1998, *ApJ*, 497, L75
- Koopmann, R. A., & Kenney, J. D. P. 2004a, *ApJ*, 613, 851
- Koopmann, R. A., & Kenney, J. D. P. 2004b, *ApJ*, 613, 866
- Kraan-Korteweg, R. C., Woudt, P. A., Cayatte, V., Fairall, A. P., Balkowski, C., & Henning, P. A. 1996, *Nature*, 379, 519
- Kronberger, T., Kapferer, W., Ferrari, C., Unterguggenberger, S., & Schindler, S. 2008, *A&A*, 481, 337
- Kulkarni, S. R., & Heiles, C. 1988, in *Galactic and Extragalactic Radio Astronomy (A89-40409 17-90)* (2nd ed.; Berlin and New York: Springer), 95
- Landau, L. D., & Lifshitz, E. M. 1959, *Fluid Mechanics* (London: Pergamon), Chap. 9
- Landau, L. D., & Lifshitz, E. M. 1960, *Electrodynamics of Continuous Media* (New York: Pergamon)
- Larson, R. B., Tinsley, B. M., & Caldwell, C. N. 1980, *ApJ*, 237, 692
- Lee, H., McCall, M. L., & Richer, M. G. 2003, *AJ*, 125, 2975
- Leon, S., Combes, F., & Menon, T. K. 1998, *A&A*, 330, 37
- Leroy, A. K., Walter, F., Brinks, E., Bigiel, F., de Blok, W. J. G., Madore, B., & Thornley, M. D. 2008, *AJ*, 136, 2782
- Lewis, I., et al. 2002, *MNRAS*, 334, 673
- Lisker, T., Grebel, E. K., Binggeli, B., & Glatt, K. 2007, *ApJ*, 660, 1186
- Lisker, T., Grebel, E. K., & Binggeli, B. 2008, *AJ*, 135, 380
- Machacek, M., Dosaj, A., Forman, W., Jones, C., Markevitch, M., Vikhlinin, A., Warmflash, A., & Kraft, R. 2005, *ApJ*, 621, 663
- Machacek, M., Jones, C., Forman, W. R., & Nulsen, P. 2006, *ApJ*, 644, 155

- Marcolini, A., Brighenti, F., & D'Ercole, A. 2003, *MNRAS*, 345, 1329
- Margoniner, V. E., de Carvalho, R. R., Gal, R. R., & Djorgovski, S. G. 2001, *ApJ*, 548, L143
- Mazure, A., Casoli, F., Durret, F., & Gerbal, D. 1998, in *A New Vision of an Old Cluster: Untangling Coma Berenices*. Proceedings, ed. A. Mazure, F. Casoli, F. Durret, & D. Gerbal (Singapore: World Scientific)
- McGee, S. L., Balogh, M. L., Henderson, R. D. E., Wilman, D. J., Bower, R. G., Mulchaey, J. S., & Oemler, A., Jr. 2008, *MNRAS*, 387, 1605
- McKee, C. F. 1995, in *ASP Conference Series*, Vol. 80, ed. A. Ferrara, C. F. McKee, C. Heiles, & P. R. Shapiro (San Francisco: Astronomical Society of the Pacific), 292
- Mei, S., et al. 2007, *ApJ*, 655, 144
- Mendes de Oliveira, C., & Hickson, P. 1994, *ApJ*, 427, 684
- Mieske, S., Hilker, M., Infante, L., & Jordán, A. 2006, *AJ*, 131, 2442
- Mieske, S., et al. 2008, *A&A*, 487, 921
- Mihos, J. C., Harding, P., Feldmeier, J., & Morrison, H. 2005, *ApJ*, 631, L41
- Minchin, R., et al. 2007, *ApJ*, 670, 1056
- Moles, M., del Olmo, A., Perea, J., Masegosa, J., Marquez, I., & Costa, V. 1994, *A&A*, 285, 404
- Moore, B., Katz, N., Lake, G., Dressler, A., & Oemler, A. 1996, *Nature*, 379, 613
- Moore, B., Lake, G., Quinn, T., & Stadel, J. 1999, *MNRAS*, 304, 465
- Moran, S. M., Ellis, R. S., Treu, T., Smith, G. P., Rich, R. M., & Smail, I. 2007, *ApJ*, 671, 1503
- Mori, M., & Burkert, A. 2000, *ApJ*, 538, 559
- Moss, C., Whittle, M., & Pesce, J. E. 1998, *MNRAS*, 300, 205
- Mulchaey J. S., Zabludoff A. I., 1998, *ApJ*, 496, 73
- Mulchaey, J. S., Davis, D. S., Mushotzky, R. F., & Burstein, D. 2003, *ApJS*, 145, 39
- Murphy, E. J., Kenney, J. D. P., Helou, G., Chung, A., & Howell, J. H. 2009, *ApJ*, 694, 1435
- Neistein, E., Maoz, D., Rix, H.-W., & Tonry, J. L. 1999, *AJ*, 117, 2666
- Niklas, S. 1997, *A&A*, 322, 29
- Niklas, S., Klein, U., & Wielebinski, R. 1997, *A&A*, 322, 19
- Nulsen, P. E. J. 1982, *MNRAS*, 198, 1007
- Oosterloo, T., & van Gorkom J. 2005, *A&A*, 437, L19
- Osmond, J. P. F., & Ponman, T. J. 2004, *MNRAS*, 350, 1511
- Panuzzo, P., et al. 2007, *ApJ*, 656, 206
- Paolillo, M., Fabbiano, G., Peres, G., & Kim, D.-W. 2002, *ApJ*, 565, 883
- Pappalardo, C., Lançon, A., Vollmer, B., Ocvirk, P., Boissier, S., & Boselli, A. 2010, *A&A*, 514, A33
- Paudel, S., Lisker, T., Kuntschner, H., Grebel, E. K., & Glatt, K. 2010, *MNRAS*, 405, 800
- Phillipps, S., Drinkwater, M. J., Gregg, M. D., & Jones, J. B. 2001, *ApJ*, 560, 201
- Phookun, B., Vogel, S. N., & Mundy, L. G. 1993, *ApJ*, 418, 113
- Pilyugin, L. S., Mollá, M., Ferrini, F., & Vílchez, J. M. 2002, *A&A*, 383, 14
- Poggianti, B. M., Smail, I., Dressler, A., Couch, W. J., Barger, A. J., Butcher, H., Ellis, R. S., & Oemler, A., Jr. 1999, *ApJ*, 518, 576
- Poggianti, B. M., Bridges, T. J., Komiyama, Y., Yagi, M., Carter, D., Mobasher, B., Okamura, S., & Kashikawa, N. 2004, *ApJ*, 601, 197
- Poggianti, B. M., et al. 2006, *ApJ*, 642, 188
- Popescu, C. C., Tuffs, R. J., Völk, H. J., Pierini, D., & Madore, B. F. 2002, *ApJ*, 567, 221
- Postman, M., et al. 2005, *ApJ*, 623, 721
- Quilis, V., Moore, B., & Bower, R. 2000, *Science*, 288, 1617
- Randall, S., Nulsen, P., Forman, W. R., Jones, C., Machacek, M., Murray, S. S., & Maughan, B. 2008, *ApJ*, 688, 208
- Rasmussen, J., Ponman, T. J., Verdes-Montenegro, L., Yun, M. S., & Borthakur, S. 2008, *MNRAS*, 388, 1245
- Rasmussen, J., Sommer-Larsen, J., Pedersen, K., Toft, S., Benson, A., Bower, R. G., & Grove, L. F. 2009, *ApJ*, 697, 79
- Rengarajan, T. N., Karnik, A. D., & Iyengar, K. V. K. 1997, *MNRAS*, 290, 1
- Roediger, E., & Brüggén, M. 2006, *MNRAS*, 369, 567
- Roediger, E., & Brüggén, M. 2007, *MNRAS*, 380, 1399
- Roediger, E., & Brüggén, M. 2008, *MNRAS*, 388, 465
- Roediger, E., Brüggén, M., & Hoeft, M. 2006, *MNRAS*, 371, 609
- Roediger, E., & Hensler, G. 2005, *A&A*, 433, 875
- Roediger, E., & Hensler, G. 2008, *A&A*, 483, 121
- Sabatini, S., Davies, J., van Driel, W., Baes, M., Roberts, S., Smith, R., Linder, S., & O'Neil, K. 2005, *MNRAS*, 357, 819
- Salpeter, E. E., & Hoffman, G. L. 1996, *ApJ*, 465, 595
- Sancisi, R., Fraternali, F., Oosterloo, T., & van der Hulst, T. 2008, *A&ARv*, 15, 189
- Sarazin, C. L. 1986, *RvMP*, 58, 1
- Schindler, S., Binggeli, B., & Böhringer, H. 1999, *A&A*, 343, 420
- Schmidt, M. 1963, *ApJ*, 137, 758
- Schoenmakers, R. H. M., Franx, M., & de Zeeuw, P. T. 1997, *MNRAS*, 292, 349
- Schulz, S., & Struck, C. 2001, *MNRAS*, 328, 185
- Sengupta, C., Balasubramanyam, R., & Dwarakanath, K. S. 2007, *MNRAS*, 378, 137

- Sivanandam, S., Rieke, M. J., & Rieke, G. H. 2010, *ApJ*, 717, 147
- Skillman, E. D., Kennicutt, R. C., Jr., Shields, G. A., & Zaritsky, D. 1996, *ApJ*, 462, 147
- Smith, G. P., Treu, T., Ellis, R. S., Moran, S. M., & Dressler, A. 2005, *ApJ*, 620, 78
- Smith, R. J., et al. 2010, *MNRAS*, 408, 1417
- Soida, M., Otmianowska-Mazur, K., Chyży, K., & Vollmer, B. 2006, *A&A*, 458, 727
- Solanes, J. M., Manrique, A., García-Gómez, C., González-Casado, G., Giovanelli, R., & Haynes, M. P. 2001, *ApJ*, 548, 97
- Spitzer, L., Jr. 1978, *Physical Processes in the Interstellar Medium* (New York: Wiley)
- Spitzer, L., Jr. 1990, *ARA&A*, 28, 71
- Stark, A. A., Knapp, G. R., Bally, J., Wilson, R. W., Penzias, A. A., & Rowe, H. E. 1986, *ApJ*, 310, 660
- Stevens, I. R., Acreman, D. M., & Ponman, T. J. 1999, *MNRAS*, 310, 663
- Stickel, M., Bregman, J. N., Fabian, A. C., White, D. A., & Elmegreen, D. M. 2003, *A&A*, 397, 503
- Struck, C. 1999, *PhR*, 321, 1
- Sulentic, J. W., Rosado, M., Dultzin-Hacyan, D., Verdes-Montenegro, L., Trinchieri, G., Xu, C., & Pietsch, W. 2001, *AJ*, 122, 2993
- Sun, M., & Vikhlinin, A. 2005, *ApJ*, 621, 718
- Sun, M., Jones, C., Forman, W., Nulsen, P. E. J., Donahue, M., & Voit, G. M. 2006, *ApJ*, 637, L81
- Sun, M., Donahue, M., & Voit, G. M. 2007, *ApJ*, 671, 190
- Sun, M., Donahue, M., Roediger, E., Nulsen, P. E. J., Voit, G. M., Sarazin, C., Forman, W., & Jones, C. 2010, *ApJ*, 708, 946
- Takeda, H., Nulsen, P. E. J., & Fabian, A. C. 1984, *MNRAS*, 208, 261
- Tanaka, M., Goto, T., Okamura, S., Shimasaku, K., & Brinkmann, J. 2004, *AJ*, 128, 2677
- Thomas, T., & Katgert, P. 2006, *A&A*, 446, 31
- Tielens, A. G. G. M., & Hollenbach, D. 1985, *ApJ*, 291, 722
- Toloba, E., Boselli, A., Cenarro, A. J., Peletier, R. F., Gorgas, J., Gil de Paz, A., & Muñoz-Mateos, J. C. 2011, *A&A*, 526, A114
- Tonnesen, S., Bryan, G. L., & van Gorkom, J. H. 2007, *ApJ*, 671, 1434
- Tonnesen, S., & Bryan, G. L. 2009, *ApJ*, 694, 789
- Tonnesen, S., & Bryan, G. L. 2010, *ApJ*, 709, 1203
- Tonnesen, S., Bryan, G. L., & Chen, R. 2011, *ApJ*, 731, 98
- Toomre, A., & Toomre, J. 1972, *ApJ*, 178, 623
- Tosa, M. 1994, *ApJ*, 426, L81
- Treu, T., Ellis, R. S., Kneib, J.-P., Dressler, A., Smail, I., Czoske, O., Oemler, A., & Natarajan, P. 2003, *ApJ*, 591, 53
- Urquhart, S. A., Willis, J. P., Hoekstra, H., & Pierre, M. 2010, *MNRAS*, 406, 368
- Valluri, M. 1993, *ApJ*, 408, 57
- van den Bergh, S. 2009, *ApJ*, 702, 1502
- van Zee, L., Skillman, E. D., & Haynes, M. P. 2004a, *AJ*, 128, 121
- van Zee, L., Barton, E. J., & Skillman, E. D. 2004b, *AJ*, 128, 2797
- Verdes-Montenegro, L., Yun, M. S., Perea, J., del Olmo, A., & Ho, P. T. P. 1998, *ApJ*, 497, 89
- Verdes-Montenegro, L., Yun, M. S., Williams, B. A., Huchtmeier, W. K., Del Olmo, A., & Perea, J. 2001, *A&A*, 377, 812
- Verheijen, M., van Gorkom, J. H., Szomoru, A., Dwarakanath, K. S., Poggianti, B. M., & Schiminovich, D. 2007, *ApJ*, 668, L9
- Vikhlinin, A., Markevitch, M., & Murray, S. S. 2001, *ApJ*, 549, L47
- Völk, H. J., & Xu, C. 1994, *InPhT*, 35, 527
- Vollmer, B. 2003, *A&A*, 398, 525
- Vollmer, B. 2009, *A&A*, 502, 427
- Vollmer, B., & Beckert, T. 2002, *A&A*, 382, 872
- Vollmer, B., Cayatte, V., Balkowski, C., & Duschl, W. J. 2001a, *ApJ*, 561, 708
- Vollmer, B., Braine, J., Balkowski, C., Cayatte, V., & Duschl, W. J. 2001b, *A&A*, 374, 824
- Vollmer, B., & Huchtmeier, W. 2003, *A&A*, 406, 427
- Vollmer, B., Thierbach, M., & Wielebinski, R. 2004a, *A&A*, 418, 1
- Vollmer, B., Beck, R., Kenney, J. D. P., & van Gorkom, J. H. 2004b, *AJ*, 127, 3375
- Vollmer, B., Huchtmeier, W., & van Driel, W. 2005a, *A&A*, 439, 921
- Vollmer, B., Braine, J., Combes, F., & Sofue, Y. 2005b, *A&A*, 441, 473
- Vollmer, B., Soida, M., Otmianowska-Mazur, K., Kenney, J. D. P., van Gorkom, J. H., & Beck, R. 2006, *A&A*, 453, 883
- Vollmer, B., Soida, M., Beck, R., Urbanik, M., Chyży, K. T., Otmianowska-Mazur, K., Kenney, J. D. P., & van Gorkom, J. H. 2007, *A&A*, 464, L37
- Vollmer, B., Braine, J., Pappalardo, C., & Hily-Blant, P. 2008, *A&A*, 491, 455
- Vollmer, B., Soida, M., Chung, A., Chemin, L., Braine, J., Boselli, A., & Beck, R. 2009, *A&A*, 496, 669
- Vollmer, B., Soida, M., Chung, A., Beck, R., Urbanik, M., Chyży, K. T., Otmianowska-Mazur, K., & van Gorkom, J. H., 210, *A&A*, 512, A36
- Vollmer, B., et al. 2012, *A&A*, 537, A143
- Walter, F., Brinks, E., de Blok, W. J. G., Bigiel, F., Kennicutt, R. C., Jr., Thornley, M. D., & Leroy, A. 2008, *AJ*, 136, 2563
- Warmels, R. H. 1988, *A&AS*, 73, 453
- Whitmore, B. C., & Gilmore, D. M. 1991, *ApJ*, 367, 64
- Whitmore, B. C., Gilmore, D. M., & Jones, C. 1993, *ApJ*, 407, 489
- Williams, B. A., Yun, M. S., & Verdes-Montenegro, L. 2002, *AJ*, 123, 2417

- Wilman, D. J., et al. 2005, MNRAS, 358, 88
- Woudt, P. A. 1998, Ph.D. thesis, University of Cape Town, South Africa
- Woudt, P. A., Kraan-Korteweg, R. C., Lucey, J., Fairall, A. P., & Moore, S. A. W. 2008, MNRAS, 383, 445
- Yagi, M., et al. 2010, AJ, 140, 1814
- Yoshida, M., et al. 2004, AJ, 127, 90
- Yoshida, M., et al. 2008, ApJ, 688, 918
- Zabludoff, A. I., & Mulchaey, J. S. 1998, ApJ, 496, 39
- Zepf, S. E., & Whitmore, B. C. 1991, ApJ, 383, 542